Journal of South American Earth Sciences
June 2023, Volume 126 Pages 104336 (24p.)
https://doi.org/10.1016/j.jsames.2023.104336
https://archimer.ifremer.fr/doc/00834/94598/

Imaging exhumed continental and proto-oceanic crusts in the Camamu triple junction, Brazil

Loureiro Afonso [1, 3, *], Afilhado Alexandra [1, 2], Schnürle Philippe [4], Evain Mikael [4], Dias Nuno A. [1, 2], Klingelhoefer Frauke [4], Gallais Flora [4], Pinheiro Joao Marcelo [4, 7], Soares José Eduardo [5], Fuck Reinhardt [5], Cupertino J.A. [6], Viana Adriano [6], Corela Carlos [1], Moulin Maryline [4], Aslanian Daniel [4], Salsa Team [1, 2, 3, 4, 5, 6, 7, 8, 9, 10]

[1] Universidade de Lisboa, Faculdade de Ciências, Instituto Dom Luiz, Lisboa, Portugal
[2] Instituto Politécnico de Lisboa, Instituto Superior de Engenharia de Lisboa, Lisboa, Portugal
[3] Agência Regional para o Desenvolvimento da Investigação, Tecnologia e Inovação, Funchal, Portugal
[4] Geo-Ocean, Ifremer, Université de Bretagne Occidentale, CNRS, 29280, Plouzané, France
[5] Instituto de Geociências - Lablithos, Universidade de Brasília, Campus Darcy Ribeiro, 70910-900, Brasília, Brazil
[6] Petrobras, Cenpes Research Center, Rio de Janeiro, Brazil
[7] Universidade Federal de Santa Catarina, Departamento de Geologia, Brazil
[8] Departamento de Geofísica, Universidade Federal do Pampa, Campus Caçapava do Sul, 96570-000, Caçapava do Sul, RS, Brazil
[9] Laboratoire Géosciences Océan, UMR6538, Université de Bretagne Occidentale, Place Nicolas Copernic, 29280, Plouzané, France
[10] Géolittomer, LETG UMR 6554-CNRS, Institut de Géographie et d'Aménagement Régional de l'Université de Nantes, Campus Tertre, BP 81227, 44312, Nantes, CEDEX 3, France

* Corresponding author : Afonso Loureiro, email addresses : afonsoloureiro@afonsoloureiro.net ; maloureiro@fc.ul.pt

Abstract :

During the SALSA experiment, in 2014, twelve combined wide-angle refraction and coincident multi-channel seismic profiles were acquired in the Jequitinhonha-Almada-Camamu, Jacuípe, and Sergipe-Alagoas basins, NE Brazil. Profile SL09 images the Almada-Camamu basin and the São Francisco craton, with 18 four-channel ocean-bottom seismometers and 22 land stations. The datasets were forward modelled and combined with pre-stack depth migration to increase the horizontal resolution of the velocity models.

Our results show that sediment thickness varies between 3.8 km in the oceanward part of the profile, 4.3 km in the Almada basin and 6.5 km in the Camamu basin. Crustal thickness at the north-western edge of the profile is of around 40 km, with velocity gradients indicating a continental origin.

The Camamu basin, which corresponds to the triple junction between the aborted N–S oriented Tucano rift, the SW-NE oriented Jacuipe-Sergipe-Alagoas branch, and the N–S Jequitinhonha-Almada branch, presents two crustal layers: a very thin upper layer, about 1.5 km thick, which increases seawards to 3 km in the Almada basin, and an higher velocity (HV) layer (6.8–7.2 km/s) about 4 km thick. This lower layer gradually disappears in the Almada basin. At the south-eastern edge of the profile, the resolution is lower

but the thickness of the crust seems to increase up to 5 km. Deep wide-angle reflections indicate upper mantle stratification.

Crustal organisation and P-wave propagation velocities in the Almada and Camamu basins indicate a transitional crust domain of exhumed continental crust affinity. In the Camamu triple junction and beneath this thin exhumed continental crust, the HV layer may probably reflect intruded materials. No exhumed upper mantle is observed along the entire profile. The easternmost part of the profile may correspond to a proto-oceanic crust. Typical oceanic crust is never imaged along the 260 km-long offshore profile.

Highlights

► The transitional domain in the Almada and Camamu basins has exhumed continental crust affinity. ► The distal basin may correspond to a proto-oceanic domain. ► Typical oceanic crust in not imaged on profile SL09. ► Necking occurs within 60 km.

Keywords : NE Brazil, South Atlantic Ocean, Passive margins, Camamu triple poin, Wide-angle refraction seismic, PSDM, Crustal structure, Cretaceous breakup, exhumed lower continental crust, SALSA

Introduction

The processes that led to the breakup of West Gondwana and the opening of the South Atlantic Ocean are still not fully understood. One of the main hindrances for an accurate reconstruction of West Gondwana is the lack of magnetic anomalies to establish a time-line for the oceanic crust-spreading rate, as the breakup occurred during the Cretaceous Normal Superchron, chiefly in the Central Segment of the South Atlantic Ocean (Moulin et al. 2010). The lack of magnetic anomalies is counterbalanced by the presence of well-marked fracture zones and lineaments that, with the knowledge of the intra-plate deformation on both Africa and South America, tightly constrain the plate movements (Moulin et al. 2010; Aslanian & Moulin 2012; Bonifacio et al. 2023).

The SALSA experiment is aimed at constraining the crustal structure and the segmentation of the NE-Brasilian margins from Jequitinhonha to Alagoas, and the geodynamical setting of the Camamu triple junction (Fig. 1), where the aborted Recôncavo – Tucano – Jatobá rift system connects with the Jequitinhonha – Almada – Camamu and Jacuípe – Sergipe-Alagoas rift systems. Here, the basins are set in with widths ranging from less than 40 km to over 200 km, and with very narrow continental shelves, which is quite rare in the passive margin settings of the eastern South American continent according to Dominguez et al. (2013). We present the results of P-wave velocity models obtained from the interpretation of a combined onshore-offshore wide-angle refraction and coincident multi-channel reflection data along profile SL09, which crosses the Camamu and Almada basins and the São Francisco craton, with a total extension of 415 km, running approximately 260 km from the continental shelf to the distal basin. This profile images the triple point of Camamu, the connection between the southern North-South trending Jequitinhonha and Almada branch with the northern Tucano failed rift and the SW-NE trending - Jacuípe and Sergipe-Alagoas branch of the rift system.

The crustal organization along the necking zone and offshore basins, as well as the nature of the transitional crust and the location of the first oceanic crust are still matter of debate in this region.

This paper continues the discussion of the basins studied during the SALSA project: Jequitinhonha (Loureiro et al. 2018) Camamu and Almada basins (this paper); the Jacuípe and Tucano basins (Aslanian et al, this issue); the Jacuípe and Sergipe-Alagoas basins (Pinheiro et al. 2018); the Almada, Camamu, Jacuípe and Sergipe Alagoas basins along profiles parallel to the coast (Evain et al., this issue).

2 Geological setting

The Jequitinhonha - Almada - Camamu (JAC) rift system extends from the Royal Charlotte bank and Cumuruxatiba basin, on the south, to the Barra and Itapuã faults, and the Recôncavo and Jacuípe basins, on the north (Fig. 1), bordering the south-eastern margin of the São Francisco craton. The basement of the Almada and Camamu basins is the Archean crust of the São Francisco craton (Schobbenhaus & de Brito Neves 2003), which is also underlain by the Itabuna branch of the

Paleoproterozoic Itabuna-Salvador-Curaçá Orogen (Delgado et al. 2003). There is no clear basement feature marking the boundary between the Almada and Camamu basins (Caixeta et al. 2007; Gontijo et al. 2007), but there are stratigraphic differences to consider them separate basins (Caixeta et al. 2007). The seaward limit between these two basins is also not always clearly defined (Menezes & Milhomem 2009). In the Almada basin, pre-rift neojurassic sediments overlay the cristaline basement, but on the Camamu basin there is an older Paleozoic sequence (Gontijo et al. 2007).

Further north, the Vaza-Barris transfer zone, a major structural fault, marks the limit between the São Francisco craton and the Paleoproterozoic Pernambuco-Alagoas Block and the Jacuípe and Sergipe-Alagoas basins (Pinheiro et al. 2018), where the N-S rift was aborted and propagated eastwards to join the Jacuípe-Sergipe rift system (Ferreira 2018) . The Camamu basin is, thus, an atypical region that borders very different geodynamical settings. The conjunction of basement heterogenities (Ferreira et al. 2009; Ferreira 2018) and the strain on the different plates and terranes resulted in a triple junction. The conjugates of the Camamu and Almada basins are the South Gabon and Congo basins respectively (Fig. 1b).

During the disaggregation of Rodinia, the São Francisco and Congo cratons were never completely detached and formed a cratonic bridge (Porada 1989; Dias et al. 2016). Neoproterozoic rifting reached the present-day Araçuaí orogen (Trompette 1997), creating the Macaúbas-Jequitinhonha basin, a gulf-like branch of the Adamastor Ocean with an undetermined extension of oceanic crust. The main Cretaceous rift trends are strongly controlled by basement inheritance, with reactivation of previous rift structures and fold belts from the Paleoproterozoic Itabuna – Salvador – Curaçá and Neoproterozoic Araçuaí-West Congo orogens (Ferreira et al. 2009; Ferreira 2018). The Itaju do Colônia and the Salvador Shear Zones are two main basement lineaments in the basement of the Camamu and Almada rift basins. These are correlated to the Taipus Mirim Accommodation Zone and the Salvador Transfer Zone, respectively. The main rift faults in the Almada basin occur N-S and with a NE-SW trend on the northern part of the Camamu basin (Ferreira et al. 2009).

Cretaceous rifting most likely started during the Berriasian-Valangian in the northern domain (Almada-Tucano region, the Congo–Camamu Basin to the Sergipe–Alagoas–North Gabon Basins) (Moulin et al. 2010; Chaboureau et al. 2013; Ferreira 2018); it finally fails at Aptian time at the Recôncavo - Tucano - Jatobá (RTJ) rift system, and propagates southwards to the Almada-Camamu and Jequitinhonha basins in several cycles of rifting and quiescence (Holz et al. 2017). During the Early Aptian, intense fault activity occurred in the Almada and Jequitinhonha basins, south of the Taipus-Mirim Accommodation Zone (TMAZ), but also on the northernmost part of the Camamu basin, forming isolated large grabens strongly bounded by basement lineaments. In the Middle Aptian, the rift architecture changed with the formation of conspicuous N-S and NE-SW hinge faults mostly concentrated in Camamu basin, north of the TMAZ. In the rest of the JAC rift system, fault activity decreased and thermal subsidence started (Ferreira 2018). Faulting and rifting propagated eastward along the JAC until marine incursions in the Early Albian marked the initial emplacement of oceanic crust (Caixeta et al. 2015).

The tightest position of the Africa and South America plates is still a matter of debate as well as the position of the oldest oceanic crust due to the lack of wide-angle data (Torsvik et al. 2009; Aslanian & Moulin 2010; Moulin et al. 2010; Heine et al. 2013; Müller et al. 2016). The syn-rift sedimentary sequences in the Paleo-Mesozoic JAC basins are bound by two major regional unconformities which, according to biostratigraphic data, indicate that the rift phase lasted about 30 Ma and ended in the Aptian/Albian transition (Küchle et al. 2005). This chronology is disputed in the Jequitinhonha basin, where the rift phase lasts only up to 5 Ma (Rangel et al. 2007; Chaboureau et al. 2013), but also in the Almada and Camamu basins, where syn-rift sediments were deposited in the Lower Aptian (Scotchman & Chiossi 2008; Chaboureau et al. 2013) or even in the Middle

Aptian (Caixeta et al. 2007; Gontijo et al. 2007). In the Camamu basin, there is a hiatus in the sedimentation, extending from Early to Middle Aptian times, with the formation of a Central Elevated Block (CEB, Fig. 1a) (Chaboureau et al. 2013), an island that formed in the Berriassian and, at its maximum size (base Valanginian), extended from the Jequitinhonha basin to the Jacuípe-North Gabon basin. The meaning of the CEB is still unclear, and Chaboureau et al. (2013) note that it records a splitting of the rift into two or three branches, changing from a narrow rift system into a wide rift system at the Vaza-Barris boundary (Pinheiro et al. (2018); Evain et al., this issue).

Salt composition, morphology and distribution in the northeastern Brazilian basins and their African conjugates, including its absence in the CEB, is quite varied (Chaboureau et al. 2013). Salt is absent in the Jacuípe basin, but there are small anhydrite and halite deposits in the Camamu-Almada basin and larger deposits in the Jequitinhonha basin. Salt deposits in their conjugate basins are larger and more homogeneous, but with a different composition from the south of the Congo basin northwards. Here, they are potassium-rich evaporites with a probable hydrothermal origin that would suggest a magmatically active extensional environment (Hardie 1990; Chaboureau et al. 2013). The same composition is also found in the Sergipe-Alagoas basin, further north on the Brazilian coast, but in almost inexpressive deposits.

The proximal part of the Camamu segment is affected by extensional faults and salt bodies (Souza et al. 2004). The Pleistocene to Barremanian sedimentary cover of these basins may reach a thickness of 8 km in the depocenters (Mohriak 2003), although along profile SL09 the maximum expected thickness is 6-7 km, according to the isopach values presented in Souza et al. (2004).

3 Data

3.1 Active Seismic data

The SALSA (Sergipe-Alagoas Seismic Acquisition) is a joint project of the Department of Marine Geosciences (IFREMER: Institut Français de Recherche pour l'Exploitation de la MER, France) and Petrobras, in collaboration with the Laboratory of "Oceanic Geosciences" (IUEM: Institut Universitaire et Européen de la Mer, France), the Faculdade de Ciências da Universidade de Lisboa (IDL, Portugal), and the Laboratório de Estudos da Litosfera, Universidade de Brasília (Brazil). The mission was conducted on the French R/V L'Atalante between April and May 2014, with the acquisition of twelve combined wide-angle refraction and high-resolution multi-channel seismics in the northeastern coast of Brazil. In this study we present the results from the SL09 profile, that crosses the Camamu and Almada Basins, with a NW-SE trending, oblique to the flowlines. It is located at the exact junction of the two northern branches of the triple junction (Tucano aborted rift, Jequitinhonha and Jacuipe-Sergipe branches), at the limit of the Salvador shear zone, and crosses the Itaju do Colônia shear zone defined by (Ferreira et al. 2009) on the base of gravity and Aptian salt isopach maps. SL09 was shot along the track of the industrial seismic profile ION GXT-2100

Profile SL09 is a 415 km long on-shore off-shore wide-angle profile orientated NW-SE (Fig. 1), comprising 18 ocean bottom seismometers (OBS) capable of recording on four channels (1 hydrophone and a 3 component geophone) and 22 land stations (LSS), each a small array of vertical short period geophones.

A 4.5 km long digital seismic streamer with 360 channels ensured the recording of near-offset multi-channel seismic (MCS) (Fig. 2). The seismic source was a tuned array of 16 air guns with a combined volume of 6544 cubic inches. A 20 km shooting gap at the SE end of the profile was due to the presence of marine mammals. The 1669 shots, spaced at every 150 m, were recorded by all instruments.

The OBS were deployed at 7 nautical miles intervals, at water depths from 810 m to 4150 m, crossing profile SL06 at the position of OBS SL09OBS13/SL06OBS27 (Fig. 1). The apparent velocity of refracted arrivals in the shallow basement vary from 5.0 km/s to 6.5 km/s. In SL09OBS15-SL09OBS16 we identify long Pg arrivals with apparent velocity of 5.2-5.6 km/s, strong PmP arrivals and Pn arrivals up to 80 km offset with large amplitudes (Fig. 3). The crossover distance between Pg and PmP arrivals is approximately 35 km. The imprint of the salt body is revealed by sharp fluctuation of apparent velocity and traveltime of all arrivals that propagate through the salt, between model distances 0 km to 30 km.

The crossover distances between Pg and PmP arrivals decreases at the SW limit of the Almada basin, indicating a crustal thickness decrease towards the distal domain (Fig. 4). Furthermore, while in the Camamu and Almada basins arrivals propagating at approximately 6.5-7 km/s are identified in almost all OBS, these arrivals no are longer recorded in the distal domain. This observation is particularly evident in Fig. 4a, when comparing both sides of the record section.

In the distal domain we observe a 50 km wide region where the basement is flatter and deeper than in the rest of the profile. Three basement arrivals can be identified in the first seven OBS (SL09OBS01 to SL09OBS07): short Pg arrivals with apparent velocity of 5.8 km/s, short and high amplitude PmP arrival and Pn arrivals up to 100 km offset with large amplitude, although with fluctuation of apparent velocity and amplitude (Figs. 5 to 7). This observation indicates a one layer crust, although another thin layer may exist.

The LSS were small arrays of vertical short-period seismometers for improved SNR and redundancy, deployed at approximately 5 km intervals. Records from the LSS are remarkably similar to each other along the whole profile (Figs. 8 to Fig. 10), indicating the absence of important lateral changes of the continental crust velocity and thickness in the São Francisco Craton. Besides Pg and intra-crustal reflected arrivals, we observe PmP arrivals and very strong Pn arrivals, up to offsets of 400 km. The existence of layering in the lithospheric mantle is evident from systematic observation of several and long branches of reflected arrivals. Station SL09LSS02 was extremely noisy and not included in the modelling.

The reflection seismic data were pre-processed with the Geocluster (CGGVeritas) software to include geometry corrections, wave equation multiple attenuation, shot-gather predictive deconvolution, time variant band-pass filter, and radon transform multiple attenuation. The OBS data were pre-processed to include clock drift corrections, and location corrections due to drift from the deployment position during their descent to the seafloor using the direct water wave arrival. Data quality was generally very good on all instruments and channels, with clear arrivals to offsets over 80 km on most instruments. Times of first and secondary arrivals where picked at their onset, without filtering whenever possible, and with band-pass Butterworth filters in all other cases.

3.2 Micro-seismic data

The active seismic data recorded by the inland stations corresponds only to the seismic waves generated by the offshore shooting, with no reverse shots. An analysis of the inland seismic record acquired during the deployment revealed micro-seismicity in the Salvador region (displayed in Brazil's epicentre maps, e.g. Bezerra et al. (2011), among others). To provide additional data in order to better constrain the onshore structure, the complete seismic records of the land stations (approximately five days) were screened for earthquake or quarry blast signals. Screening was performed with daily spectrograms (Vales et al. 2014) to identify coherent signals. These were later analysed with SEISAN (Havskov & Ottemöller 1999) to obtain a preliminary hypocentral location. All distant events were excluded, leaving 72 regional or local events at varying depths (Tab. S3, Fig. S25, supplementary material), corresponding to quarry blasts or small earthquakes. Only events

recorded in at least 15 stations and within 10 km of the profile were considered for further evaluation.

On profile SL09, one of the identified events was recorded in all seismic stations, with clear P, S and Rg arrivals. For a P-wave propagation velocity of 6.15 km/s and vP/vS of 1.746, the epicentre is at W38.98740 S13.00614, with an RMS of 150 ms for the propagation time (orange star in Fig. 25, supplementary material). This event was included in the modelling.

4 Methods

4.1 Forward modelling

The wide-angle OBS data were modelled using the RAYINVR (Zelt & Smith 1992; Zelt 1999) software package using a layer stripping-approach and iterative damped least-squares travel-time inversion at later stages. The starting parametrization for each layer was defined by screening all instruments for the most important features, either strong reflections or clear turning waves and critical refractions (Figs. 5 to Fig. 10). To avoid over-parametrization, only the interfaces discernible in the OBS data were included in the models. Arrival times of near-offset reflections were picked from the MCS data for the main sedimentary interfaces (Fig. 2) that were also identifiable on the OBS data. These arrival times were converted to depths using the propagation velocities obtained from the OBS data. Depth and velocities of the crustal layers and the upper mantle were modelled using exclusively the OBS and LSS data. Velocity gradients, relative amplitudes, and cut-off points were constrained by comparison of synthetic seismograms with the record sections (Fig. 5a and Fig. 5b; or Fig. 7a and Fig. 7b, for example).

Keeping in line with the minimum structure modelling approach (Zelt & Smith 1992), interface depth and velocity node spacing were included as needed to model lateral variations of the seismic velocity field and without introducing complexity not required by the data.

The final model for SL09 (Fig. 11) shows the velocity field and interface geometries of all the main sedimentary layers and basement. On this profile, eight sedimentary layers were modelled, reaching a maximum thickness of 6.5 km in the Camamu basin, 4.3 km in the Almada basin and 3.8 km in the distal basin 3.5 km. The modelled onshore sedimentary basin has a thickness of less than 1 km. The sediments generate near-offset reflected arrivals having zero offset arrival times coherent with the interfaces interpreted in the MCS data. Refracted arrivals have apparent velocity in the range 2.0-3.0 km/s in layers S1 to S4, 3.0-3.5 km/s in layer S6, 4.0 km/s in layer S7 and 4.5-5.0 km/s in layer S8. The velocities at the top of the layers are very well-constrained, with the vertical velocity gradient established from cut-off distances and relative amplitudes. The velocities in the sedimentary layers are further confirmed by the analysis of the residual move-out of a pre-stack depth migration of the MCS data.

At shallow levels, the limit between Necking and Camamu domains coincides with the outer limit of salt and extensional tectonic faults in the centre of the Camamu basin. This limit is marked at depth by a flattening and an important decrease of velocity contrast across the Moho. This effect is due to the existence of a 2.5-4 km thick lower crust layer with a propagation velocity of 6.55-7.15 km/s and a velocity gradient that decreases oceanward from 0.25 km/s/km to 0.1 km/s/km in the Camamu domain. This layer is overlain by a very thin layer (1-1.5 km thick) that has velocities in the range of uppermiddle-continental crust velocity (6.0 to 6.3 km/s and a high velocity gradient of 0.2 km/s/km.

In the Camamu domain, the nature and continuity of the lowermost sedimentary layer is uncertain (Fig. 11). This layer, which he named layer U, can include one or several materials such as sedimentary deposits, volcanics, mass waste deposits or exhumed material at its base. This layer

reaches a maximum thickness of 2.5 km with velocities of 4.75-4.85 km/s. The interface between this layer and the first crustal layer generates wide-angle reflected arrivals along its fullest extent, making it very likely that it marks an important lithological contrast, either the top of basement or an intra-crustal interface.

On the São Francisco craton, four basement layers were modelled, based on the different refracted and reflected arrivals: upper crust, middle crust, lower crust, and lithospheric mantle. The middle and lower crust thin out under the Camamu basin. From the necking zone towards the distal basin, the basement structure is modelled as five layers: upper crust, High Velocity zone (HV) and three intra mantle reflectors. The upper continental crust is present across the São Francisco craton, and the Camamu and Almada basins, with a maximum thickness of 16 km on the craton, thinning to 6 km in the Camamu basin and then to less than 2 km in the Almada basin until it pinches out at the basin limit. The middle continental crust is present in the São Francisco craton, with a maximum thickness of 13 km, thinning out under the Camamu basin. The lower continental crust is only present under the craton, with a maximum thickness of about 12 km.

In the Almada and distal basins, the top of basement is well-marked by a typical alignment of strong diffractions. The wavelength of basement roughness is about 10-20 km, defining depressions of approximately 0.5 s twt in the Almada basin; towards the distal basin the basement deepens approximately 1 s twt and becomes flat. An abrupt change occurs when crossing the shear zone from Almada to Camamu basin, where the top of basement becomes hard to identify exclusively from the MCS data alone.

A lower crustal unit appears at the transition between the Camamu and Almada basins and extends into the distal domain. It reaches a maximum thickness of 4 km in the middle of the Almada basin and progressively thins out to the SE of the profile.

Several intra-mantle reflections are apparent on the seismic data and were modelled accordingly. The lithospheric mantle has a propagation velocity of 8.4 km/s 50 km below the Moho to provide a gradient capable of explaining the observed refracted arrivals.

The model for SL09 is able to justify around 83% of the picked travel-times, with a pick uncertainty of 100 ms. The model is well adjusted, with a normalized χ^2 value of 2.623 (Tab. 1).

4.2 Gravity modelling

During the cruise, filtered gravity data were acquired every 10 s using a Lockheed Martin BGM-5 dynamic gravimeter installed as close as possible to the centre of gravity of the vessel. This gravimeter additionally calculates the Eötvös correction, and the Free Air and Bouguer gravity anomalies. The data were merged with the navigation data and corrected for instrumental drift using the Caraïbes software, developed by Ifremer. Gravimeter drift was corrected using three measurements at absolute gravity points in Maceió, São Paulo and Salvador. Outliers were manually cleaned. The precision of the measurements is evaluated at 1 mGal. The gravity anomaly data was extended inland with Free air gravity derived from satellite data (Sandwell et al. 2014). The observed gravity is relatively smooth, with a positive anomaly on the edge of the continental shelf, and a negative anomaly in the necking zone. An estimate of crustal density can be obtained by correlating the acoustic wave propagation velocities with rock densities (Christensen & Mooney 1995). Although there is no absolute relationship between acoustic propagation velocity and density, gravity modelling shows that the seismic model is compatible with the measured gravity anomaly. Areas of the model unconstrained or poorly constrained by seismic data can be further constrained as a first order interpolation by gravity modelling.

For profile SL09, we built a 2D model with homogeneous density blocks (Fig. 12a), by conversion of seismic velocity to density according to Ludwig et al. (1970). The sedimentary units have, thus, densities ranging from 1800 kg/m³ to 2500 kg/m³. Basement densities range from 2700 kg/m³ to 2900 kg/m³. The regional component of the free-air anomaly indicates an increase of mantle density towards the continent. To fit this regional component, we adjusted the density of three basement blocks within 5% of the density-velocity relation. The density was set to 3180 kg/m³ and to 3240 kg/m³, in the layers where Pm1P and Pm2P propagate, representing reductions of 3.6% and 3.0% respectively. In the B5 unit, the density was reduced by 1.5% to 2900 kg/m³. The density of the salt block (pink region in Fig. 12a) was set to 2180 kg/m³. To avoid edge effects, the density model was extended 400 km to each side and up to a depth of 100 km, where isostatic compensation may be reached.

The density conversion of our velocity model (Tab. 2) is able to predict the main trend of the gravity anomaly (Fig. 12b). The calculated gravity anomaly fits the observed values with a 16 mGal RMS. The largest difference between observed and calculated gravity anomaly, 27 mGal (Fig. 12b), occurs at the NE limit of the salt body, which is not constrained by seismic data. The calculated gravity anomaly is also consistent with the satellite-derived gravity values observed on parallel profiles extracted north and south of the profile at 10, 20, and 30 km.

In the Almada and distal basins, the lithospheric load is within acceptable ranges for a crust in isostatic equilibrium (Whitmarsh et al. 1996). The load increases towards the continent in the Camamu basin, reaching a local maximum over 200 Bar (Fig. 12c) at the fault that limits the salt to the SW. From this point to the NW it decreases, indicating that shear stress larger than those supported by an isostatic equilibrated crust may exist. Since both faulting and recorded seismicity are present in the the zone, Airy isostasy is certainly not applicable, thus there is no violation of the fundamental laws of mechanics. The densities for the upper mantle must be consistent with the geological setting, but in this complex region, with Archean and Proterozoic units and at the northern limit of the Neoproterozoic rifting, several hypotheses are possible. The modelled mantle densities are consistent with a moderately depleted Archean Sub-continental lithospheric mantle (SCLM), that can have mean densities as low as 3310 kg/m³; or a depleted Proterozoic mantle, with mean densities as low as 3330 kg/m³ (Poudjom Djomani et al. 2001).

4.3 PSDM RMO

To verify the accuracy of the final velocity model, the MCS data of the profile were pre-stack depth migrated (PSDM), and a residual move-out analysis was performed, using the Seismic Unix package (Stockwell 1999; Cohen & Stockwell Jr. 2015). The final velocity layered model was converted to a 50 x 25 m spaced grid, and used to compute travel-time tables regularly spaced at 150 m (the same spacing as the recorded shots) along the profile by paraxial ray tracing. Solving the eikonal equation compensates travel-times in shadow zones. The travel-time tables are used to calculate a common offset Kirchhoff depth migration. Migrated traces are output as common image gathers (CIG) binned at 25 m, with 30 offset-classes between 249 and 4596 m, spaced at 150 m. SALSA09 (Fig. 13a) was migrated up to a depth of 12 km, showing very good resolution in the sedimentary layers, with good agreement between strong reflectors and their wide-angle estimated depths.

Calculating the residual move-out (RMO) allows a dip-independent velocity analysis on the migrated CIG. This implies that, if the velocity model is close to the true medium velocity, all common offset migrated panels map the recorded seismic events to the same reflector depth. If the velocity model significantly deviates from the true medium velocity, the move-out from near to far offset translates into an interval velocity correction (Liu & Bleistein 1995). Additionally, depth migrated gathers are excellent records of amplitude variations with offset, and therefore are indicators of in-situ rheological changes. The residual move-out behaviour coupled with the seismic

character from PSDM images are key elements to locate accurately major geological contacts, moreover with higher horizontal resolution when compared to the OBS records.

The RMO analysis of the migrated SALSA09 (Fig. 13b) section shows mostly sub-horizontal arrivals, indicating a good agreement between the modelled and true medium velocities in the entire sedimentary basin and upper crust. Coherence is lost immediately below the basement, due to the arrival of the free surface multiples.

5 Model evaluation

5.1 Indirect model evaluation

Models are evaluated not only by the number of justified observations and global data fit, but also by the uniformity and density of their ray coverage, smearing, resolution and the number of rays that constrain each node (hit counts).

Most interfaces of the SL09 model are reflective (Fig. 14a) in segments longer than 50 km, indicating that acoustic impedance contrasts do not vary significantly in this range of distances along the interfaces. As a consequence, the depth nodes have a large number of hit-counts (Fig. 14b) and are well resolved (Fig. 14d) with little smearing (Fig. 14c).

In the sedimentary cover, we observe a lateral variation of the velocity related to the limits of the basins, with each layer including a few velocity nodes, but still they are generally well resolved and not smeared. The less well-resolved velocities in the sediments occur in the salt domain, nevertheless, the resolution is still within the limits of well resolved parameters and its smearing is acceptable. The lowest values of resolution are attained in the middle and lower continental crust and in the lower crustal unit that is only present in the SE extremity of the model. However, the velocity of upper and middle continental crust and the mantle bellow the salt are most probably smeared, meaning that there is a dependence among these velocities (the data is not able to resolve each velocity independently of the others).

The top of basement is reflective almost everywhere, indicating a good constrain of this interface, in good agreement with its high resolution values and little smearing, although having less hit counts than other deeper interfaces. Similarly, the Moho continuously generates PmP arrivals in Camamu and Almada Basins and in the distal basin. The region of thinning of the lower continental crust, from the limit of the intra-cratonic basin to the hinge line, is also reflective. Besides the Moho, two intra-mantellic interfaces at depths of 30 km to 40 km generate reflected arrivals. The deeper intra-mantellic interface, lying at 55 km to 40 km depth, is continuously followed below the Intracratonic basin, Camamu and Almada.

All layers show large hit-counts, indicating that the velocities are well constrained. Hit-counts for interface depths are larger than 1000, indicating a good constraint also on interface depths and topographies. Smearing is higher on the NW edge of the model, mostly due to the lack of reverse shots to better constrain the geometry. Nevertheless, the smearing values suggest that the model is not over-parametrized.

5.2 Uncertainty estimation using VMONTECARLO and model uniqueness

The velocity model suggests the disruption of the deepest layer in the crust, disappearing towards the south-east, between the Almada and distal domains, and towards the north-west, between the Camamu and Necking domains. In order to assess the reliability of alternative models not comprising these features, we performed a series of tests, generating 49968 valid random models with VMONTECARLO (Loureiro et al. 2016), using the Metropolis algorithm and adaptive

variance to increase the convergence. These tests also provide important limits to interpretation, since they establish bounds for velocity and velocity gradient. The SL09 model was preprocessed, in order to obtain a suitable model for random parameters generation, including horizontal and vertical limiting, pinchouts and linearly dependant parameters removal. We allowed for maximum velocity fluctuations of ± 0.60 km/s and maximum interface depth fluctuations of ± 2 km. We used both a Fisher hypothesis test and score based comparisons (Loureiro et al. 2016) to filter the random models according to the required level of data fit, that should be similar to the obtained for SL09 model. The preferred SL09 model is capable of tracing 14343 rays to 16372 picks (justifying 87% of the data), with an RMS of 0.11 s, a χ 2 of 1.20, and a VMONTECARLO score of 0.86.

For SL09, 55 models had better score than the preferred model, and from these, 13 also had better RMS, χ^2 value and number of justified observations. The best random model is capable of tracing 14712 rays (justifying 90.0% of the data), with an RMS of 0.11 s and a χ^2 of 1.13.

In the Necking Domain, the results indicate that the lower crust may be up to 1.5 km thicker with a velocity gradient smaller than the velocity gradient of the preferred SL09 model (Fig. 15). In fact this is also true in the Camamu Domain, where the bounds of velocity uncertainty in the lower crust allow for a velocity gradient decrease, namely considering the best random model. Similarly, the results suggest that a thin lower crust layer may occur in the distal domain (Fig. 15), probably up to 2 km thick.

The global uncertainty map for profile SL09 (Fig. 15a and Fig. 15b) shows that the crustal layers are generally well constrained, with very localized defocusing effects.

5.3 Comparison with GXT

SALSA09 was shot along the track of a still not published seismic acquisition line, profile ION GXT-2100. This dataset provides additional constraints to the sedimentary basin and crustal structure and has higher penetration than the SALSA09 MCS record section. The reflective and transparent pockets in layer U are well marked in both SALSA09 and GXT-2100, having no significant vertical mismatch. The layer with velocity 6.0-6.3 km/s, transparent in the Camamu domain, presents pockets of reflectors in the Almada and distal domain. On the line drawing of this profile there are several deep crustal reflectors that appear to be a highly reflective Moho. In the north-western-most Camamu domain, this thick reflective band coincides with the whole lower-crust, contrasting with the transparent continental crust in the Necking domain. Due to the spacing of the instruments, refraction data are typically unable to retrieve small reflector wavelengths, but the final velocity model of SL09 is capable of bounding most of the major units identified in the ION GXT-2100 profile with a good agreement (Fig. 16). The deep reflectors in the distal basin identified on the GXT profile (red question mark on Fig. 16) are not visible in the wide-angle data and thus not modelled. However, the LSS data shows reflections below the Moho, indicating a possibly layered mantle, and this pack of reflectors may mark the base of a shallower high velocity mantle layer.

6 Discussion

In order to characterize the P-wave seismic velocity variations along profile SL09, 1-D velocity-depth profiles were extracted from the velocity model at 10 km interval (Fig. 17), allowing to discuss the properties of crust and to establish the lateral segmentation along the profile Based on these 1-D velocity depth profiles, we identify five main regions along the profile from north-west to south-east: the São Francisco Craton, the Necking domain, the Camamu domain, the Almada domain and the distal domain (Fig. 17a).

6.1 Nature of layer U

Between the reflector S8 (light green line on Fig. 2) and the basement top B1 (light blue), MCS data indicates the presence of an about 1 sec TWT thick layer U. The nature and continuity of this layer is unclear.

According to model evaluation results (Fig. 14), whilst the depth of the base of this layer is very well resolved by the data, the velocity of this layer is less well resolved than the velocity of the remaining layers in this domain. Thus, its velocity and velocity gradient ranges can be larger than the given values and its nature (substratum or sedimentary) remains in question (Fig 18: igneous nature in light orange, sedimentary nature in dark bands). However, even taking into account the results of the uncertainty estimation and comparing the velocity depth profiles in the Necking and Camamu domains, the crust underlying Unit U, with velocities above 6 km/s, cannot be considered as the same envelope.

Although the velocity range in the anomalous velocity layer U is similar in the Necking Domain and in the Camamu Domain, a speculative hypothesis would be to consider a similar lithology of this layer on both domains. The MCS data suggests (Fig. 2) a basement small-scale relief beneath the base of S8, configuring grabens filled with a thin sedimentary cover in the Camamu domain, and the Vzs profiles in Camamu basin present an inversion of velocity, not observed in the necking zone, suggesting the presence a magmatic sub layer in that area. In another hand, the gravity modelling requires a lower density for the U layer in the Necking domain, which is consistent with the presence of a salt body or a mixture of salt and sediments of unknown thickness.

Layer U is therefore considered as a mixture of of salt and sediments in the necking zone, moving to a more volcano-sedimentray layer in Camamu Basin according to the results on the perpendicular profile which crosses the Jacuipe Basin (cf. Evain et al., this issue). The PSDM (Fig. 13) confirms this interpretation and shows that layer U has internal structure, with contrasting thick reflective pockets and transparent highs, indicating that layer U is not a single unit.

The base of the basin therefore shows a rather sharp increase of depth in the Camamu area compared to the surrounding areas, giving it a “boutonnière” type shape.

6.2 Unthinned continental crust domain

The São Francisco craton, up to approximately 50 km model distance, shows a 41 km-thick unthinned continental crust, compatible with previous results that indicated a total crustal thickness between 37 and 41 km for this region (Assumpção et al. 2013). Here, the crust has propagation velocities, gradients and layer thicknesses comparable to those of shields, extended continental crust, and rifted continental crust (Fig. 19). A long deep-seismic refraction sounding transect, crossing the Borborema Province and the Tucano Graben (Soares et al. 2010; Tavares et al. 2012; de Lima et al. 2015) enters the Serrinha block in a direction approximately N-S, and ends 90 km north of SL09. This transect reveals a two-layer crust with a total thickness of 39 km to the south of Tucano. The upper crust is 18 km thick with velocity 6.1-6.2 km/s and the lower-crust is 21 km thick with velocity 6.9-7.0 km/s (Lopes & others 2017). Our modelling of SL09 shows a similar total crust thickness, but organized into three layers: an upper crust 16 km thick with velocity 6.1-6.2 km/s, a middle crust 13 km thick with velocity 6.25-6.35 km/s, and, at 30 km model distance, a lower crust 11 km thick with velocity 6.85-7.15 km/s.

When compared with the results from profile SL02 (Pinheiro et al. 2018), on the Sergipano Fold Belt (Fig. 19a), it is evident that the crustal organization is very different on each side of the Vaza-Barris transfer zone, highlighting the contrasting tectonic heritage of both segments (see also Evain et al., this issue). The total crustal thickness in the São Francisco Craton is larger than in the

Sergipano Fold Belt (36–41 km compared to 27–36 km) and the upper crustal layer is also much thicker in the craton (26–29 km compared to 4–8 km).

570

6.3 Necking domain

On the necking domain, the continental crust thins from 40 km at -30km model distance to about 6 km at 30 km model distance. The continental characteristics of the crust become less clear as we move towards the Camamu basin, showing a very abrupt 34 km thinning of the crust in a distance
575 of approximately 60 km. There are also striking differences when compared to the necking domain in the Sergipe-Alagoas passive margin (SL01 and SL02, Fig. 20).

6.4 The Camamu, Almada and Distal domains

580 In the Camamu, Almada and distal domains, Romito and Mann (2022), based on multi-channel seismic, gravimetric and magnetic data analysis and interpretation, divide the transitional crust domain into three sub-domains. They define their Domain 2 as a 20 km-wide zone of exhumed mantle, which may correspond to a projection into the Almada Basin. Profile SL09 crosses their Line A profile between OBS 5 and 4, between 165 et 175 km model-distance, within their domain 3
585 interpreted as a proto-oceanic crust.

Exhumed mantle at the ocean-continent transition zone is characterized by high P-wave velocities at shallow depths and the absence of an oceanic Layer 3 and Moho step. These characteristics are usually enough to distinguish it from thinned continental crust, oceanic crust or magmatically
590 underplated crust (Minshull 2009). However, velocities increasing rapidly to more than 7.6 km/s within a few kilometres of top basement can also indicate anomalously thin oceanic crust (Mutter & Mutter 1993; Funck et al. 2003).

To test the hypothesis of mantle exhumation, the 1D velocity-depth profiles extracted along the
595 Almada and Distal basin were compared to similar profiles extracted from wide-angle seismic models (Figs. 21a, 21b, 21d and 21e) in the Newfoundland Grand Banks margin, Iberia Abyssal Plain, and southern Galician margin, where the ocean-continent transition zones have been interpreted as exhumed mantle, serpentinized upper mantle, or a mixture of both. In the southern Galician margin serpentinized upper mantle and lower continental crust materials were drilled
600 during Legs 173 and 149 of the Ocean Drilling Program (Chian et al. 1999), with the lower continental crust materials being interpreted as rafts that float in an overall upper mantle exhumation regime that occurs along a deep detachment (Boillot et al. 1987; Manatschal et al. 2001). The 1D velocity-depth profiles are also compared to a compilation of mean velocity-depth variations in the ocean-continent transition (Fig. 21b and 21e, Minshull, 2009) in the UK western
605 approaches margin, where an anomalously high Vp/Vs ratio indicates the presence of strongly serpentinized rocks (Bullock & Minshull 2005).

The velocity structure of the Almada Basin up to the distal domain of profile SL09 is noticeably different from that of the profiles in the North Atlantic, where the basement is presumably formed
610 of exhumed mantle. Although there are high P-wave propagation velocities at shallow depths, the gradients are much less pronounced. Furthermore, the 1D velocity-depth profiles show a strong velocity jump between 6.3-6.8 and 8km/s, representing a clear Moho boundary. These differences invalidate the presence of exhumed mantle in the Almada and Distal basins.

615 Our modelling results show a upper crustal unit in the Camamu and Almada basins with P-wave propagation velocities ranging between 5.8 and 6.35 km/s, compatible with middle to lower continental crust. Below that unit, a lower unit of high velocities (HV zone), ranging between 6.55 and 7.15 km/s (Fig. 11) appears along the Camamu basin and gradually thins out until it disappears in the Almada basin. This HV zone may be compatible with intruded continental crust and/or

altered or serpentinized mantle. The Vz profiles present anyway two strong steps of P-wave propagation velocities that preclude a continuous serpentinization process. Moreover, the high density of this unit (Fig. 12) excludes high degrees of serpentinization (Mével 2003), which indicates a non-mantelic origin. The internal reflectivity, apparent in the GXT-2100 line drawing (Fig. 16), is also in favour of a crustal nature (Hammer & Clowes 1997; Cook et al. 2010), and the reflection at the bottom of this layer may be a good candidate for the seismic Moho (Prodehl et al. 2013).

To test the exhumed lower continental crust hypothesis, we compared the 1D velocity-depth profiles in the Camamu, Almada and distal domains with those extracted from the wide-angle models in Brasilian and Mediterranean margins areas, where exhumed lower continental crust is proposed (Fig. 22). Despite some notable differences in the velocity crustal structure of the Camamu and Almada basins, their Vz profiles are all compatible, in terms of velocity gradients, to those from regions where exhumed/intruded lower continental crust is proposed.

The Almada basin has a rougher basement topography, when compared to the neighbouring domains, which could indicate an oceanic nature with a slow spreading rate or lower mantle temperatures. 1D velocity-depth profiles across these domain were compared with a compilation of Atlantic oceanic crusts of similar age (White et al. 1992) and a compilation of oceanic crusts (Christeson et al. 2019). (Fig. 23b) and to Vz-profiles of domain interpreted as proto-oceanic crust (Fig. 21f). The crustal organization from the Camamu basin onwards is inconsistent with typical oceanic crust or proto-oceanic crust in terms of top velocity, propagation velocities, gradients and layer thicknesses. The Almada basin is also likely comprised of exhumed lower continental crust (Fig. 22b).

In the Camamu and Almada basins, the bottom of the lower HV layer coincides with a high-amplitude more or less undulating reflector identified in cyan in the line-drawing of profile ION GXT2100 (Fig. 16). This reflector shares similarities with the “M-reflector” proposed by Blaich et al. (2010) for this region. The wavy character of deep reflectors is also found in the conjugate margin, for example in profile PROBE23 (Rosendahl et al. 1991). In the Middle South Gabon Basin, a similar undulating reflector is also identified, the “G-reflector” (Dupré et al. 2011). The “G-reflector” appears also at approximately 10 s twt, and is interpreted as the transition between an upper crust and the result of mafic intrusions of the continental crust that has been thinned during extension.

A possible interpretation for this unit is that the lower continental crust, as it is thinned, is intruded by magmatic material, begins to flow (Bott 1971; Buck et al. 1999; Aslanian et al. 2009) and forms lithospheric-sized boudins. A similar mechanism has also been proposed for the closely-related Jequitinhonha basin (Rangel et al. 2007) and the Uruguayan margin (Clerc et al. 2015).

The steep deepening of the base of the Camamu basin, which gives it a “*boutonnière*” shape, the very thin upper crustal layer and the HV underlying layer interpreted as intruded material, may be linked to its very specific location at the junction of the three branches in action in the region at the time of rifting: this triple junction area recorded both movements of São Francisco plate and Africa plate with respect to the Tucano sub-plate, which produced respectively the Recôncavo-Tucano-Jatobá rift and the Jacuípe-Sergipe-Alagoas margin at Berriasian-Valangian time (Moulin et al. 2010; Chaboureau et al. 2013).

6.6.1 The distal domain

The distal domain, between the Almada basin and 200 km model distance, shows a single basement layer, with P-wave propagation velocities ranging between 5.8 to 6.35 km/s and a strong step at the Moho boundary (dark purple lines in Fig. 21a-c, 22c and 22f, 23c). This crustal velocity structure is

incompatible with normal oceanic crust (Fig. 23c) or exhumed serpentinized upper mantle (Figs. 21a & b), but is consistent with a proto-oceanic (Fig. 21c) or a very thin exhumed continental crust (Fig. 22c). The most distal domain (from 200 km model distance onwards, light profiles in the figures), where no OBS were deployed and therefore less constrained, presents Vz-Profiles very similar to the ones observed on the proto-oceanic crust of the Pará-Maranhão/Barreirinhas margin (Fig. 21c, Aslanian et al., 2021; Moulin et al., 2021). On profile SL09, the true oceanic crust was never reached, which is coherent with the results on SL11 and SL12 profiles (Loureiro et al. 2018).

7 Conclusions

Profile SL09 images a narrow margin, with the complete necking of the continental crust occurring within less than 60 km (Fig. 20). The transitional domain in this region is in general agreement with the transitional domain proposed for the same area by Blaich et al. (2008), including the density of the lower crustal body, but not in the position of the Continent-Ocean Boundary, which is never reached on profile SL09.

Seismic velocity gradients and crustal organization discard a serpentinized upper mantle provenance for Domain 2, proposed by Romito and Mann (2022) (green arrow on Fig.17a) .The transitional domain is most probably composed of exhumed continental lower crust, similarly to what is found in the Jequitinhonha basin (Loureiro et al. 2018), immediately south of this profile. In the Camamu margin and partly in the Almada margin, there is an anomalous velocity zone that underlays the lower crust and bounds high-amplitude reflectors. The seismic propagation velocities and the depth of the reflectors suggest oceanward creep of the lower crust linked to the crustal thinning process, as proposed southwards for profile SL11 (Loureiro et al. 2018), but also in other margins: the Pará-Maranhão/Barreirinhas passive margin (Aslanian et al. 2021), the Angola Margin (Contrucci et al. 2004; Moulin et al. 2005; Aslanian et al. 2009), the Mediterranean margins (Afilhado et al. 2015; Moulin et al. 2015), the NW Greenland margins (Guan et al. 2019), the North Colorado margin (Shuck et al. 2019; Bécel et al. 2020), the margins of the austral segment of the South Atlantic ocean (Chauvet et al. 2021). The apparent imbrication of the domains reinforces the idea that the lower continental crust flow is gradually recrystallized to build a first proto-oceanic oceanic crust(Bott 1971; Aslanian et al. 2009; Sibuet et al. 2012; Afilhado et al. 2015; Aslanian et al. 2021; Moulin et al. 2021), leading to complete continental mantle erosion before the first typical oceanic crust appears (Bécel et al., 2020).

These results are included in the Fig. 24, which presents a compilation of all results acquired during the SALSA experiment (Loureiro et al. 2018; Pinheiro et al. 2018; Aslanian et al. ; Evain et al.) and the compilation done by Assumpção et al. (2013) on land.

The crustal thicknesses of the unthinned crust along the SALSA profiles are coherent with the onshore compilation of Assumpção et al. (2013), showing the Vaza-Barris transfer zone as a major structural fault, which marks the limit between the São Francisco craton and the Paleoproterozoic Pernambuco-Alagoas Block, on one side, and the Jacuípe and Sergipe-Alagoas basins, on the other side, as already noticed by Pinheiro et al. (2018). Along the entire system, the width of necking zones (thick dashed black lines in Fig. 24) present two strong variations: 1) between the Jequitinhonha and the Almada Basins, to the south, and 2) on either side of the Vaza-Barris transfer zone, to the north between the Jacuipe and Sergipe margins, showing the impact of the tectonic heritage on the structure of the margin (Evain et al.). The domain just after the necking zone presents a rather similar crustal thickness in entire system of about 10km, except in the Camamu Basin, along profile SL09, which presents a thinner basement, probably due to the evolution of the triple junction. This triple junction is marked by a structure “en boutonnière” and an anomalous velocity zone that underlays the lower crust and that expands east-northwards in the Jacuípe margin, probably connected to the Africa Plate movement (Evain et al.).

Whilst in the Jacuípe-Sergipe-Alagoas margins the oceanic crust is always rapidly reached, this is not the case in the southern Margins, southwards of the Camamu triple junction, where the intermediate domain is likely of exhumed lower continental nature. This difference may represent a different geodynamical evolution but the connection between the two areas is not imaged. No exhumed upper mantle is observed in the entire area, but some very small occurrences may exist and not be imaged within the resolution of the wide-angle data.

7.1 Acknowledgements

We thank Dr. Pedro Kress and an anonymous reviewe for their excellent suggestions and feedback, and their constructive and exhaustive reviews that significantly improved this manuscript.

We are indebted to the captain, crew, and MCS technical team of the R/V L'Atalante. We also thank J. Crozon, P. Fernagu, P. Pelleau and M. Roudaut, the OBS technical team, and J. Soares, R. Fuck, M. Lima, J. Pinheiro, F. Lima, M. Sobrinho, P. Resende, R. Oliveira, N. Dias, C. Corela, J.L. Duarte, A. Loureiro and D. Alves, the land stations deployment team.

The GMT (Wessel & Smith 1998), Seismic Unix (Stockwell 1999; Cohen & Stockwell Jr. 2015), and Geocluster (CGG-Veritas) software packages were used extensively in the preparation of this paper. R. Fuck acknowledges CNPq, Brazil research fellowship (30.1065/2016-0) and INCT Estudos Tectônicos research grant (46.5613/2014-4). Afonso Loureiro acknowledges funding from the Portuguese Fundação para a Ciência e a Tecnologia (FCT) I.P./MCTES through national funds (PIDDAC) – UIDB/50019/2020.

7.2 Author contributions

The SALSA Project was led by D. Aslanian and M. Moulin, from Ifremer, and A. Viana, from Petrobras. Processing of the high resolution seismic data was done by A. Baltzer, M. Benabdellouahed, and M. Rabineau. The hypocentral determination was done by I. Rio. The geodynamic interpretations were done by D. Aslanian and M. Moulin. Modelling of profiles SL11 and SL12 was done by A. Loureiro. Modelling of profile SL10 was done by F. Klingelhöfer. Profile SL09 was modelled by A. Afilhado and jointly interpreted by A. Loureiro. F. Gallais modelled profiles SL07 and SL08. M. Evain modelled profiles SL05 and SL06. Profiles SL01 and SL02 were modelled by J. M. Pinheiro. Modelling of profiles SL03 and SL04 and processing of the deep-sounding reflection seismic data was done by P. Schnürle. S. Gonçalves applied RTM to profile SL04. This article was written by A. Loureiro, based on the original draft from A. Afilhado.

The Salsa Team is composed by: Morvan, L., Mazé, J.P., Pierre, D., Roudaut Pitel, M., Rio, I., Alves, D., Barros Junior, P., Biari, Y., Corela, C., Crozon, J., Duarte, J.L., Ducatel, C., Falcão, C., Fernagu, P., de Lima, M. V., Le Piver, D., Mokeddem, Z., Pelleau, P., Rigoti, C., Roest, W. & Roudaut, M..

Reference list

Afilhado, A., Moulin, M., Aslanian, D., Schnürle, P., Klingelhoefer, F., Nouzé, H., Rabineau, M., Leroux, E. & Beslier, M.-O. (2015). Deep crustal structure across a young passive margin from wide-angle and reflection seismic data (The SARDINIA Experiment) – II. Sardinia's margin. *Bulletin de la Société Géologique de France*, 186, pp.331–351. DOI:10.2113/gssgfbull.186.4-5.331.

Aslanian, D., M. Evain, P. Schnurle, A. Loureiro, M. Moulin, N.A. Dias, & Afilhado, A. (this issue). From São Francisco Craton to Jacuípe basin, passing trough the South Tucano and Recôncavo grabens: new insights from wide-angle-MCS data. *Journal of South American Earth Sciences*.

Aslanian, D., Gallais, F., Afilhado, A., Schnurle, P., Moulin, M., Evain, M., Dias, N.A., Soares, J., Fuck, R., Neto, O. & Viana, A. (2021). Deep structure of the Pará-Maranhão/Barreirinhas passive margin in the equatorial Atlantic (NE Brazil)". *Journal of South American Earth Sciences*, 110, p. 103322. DOI:10.1016/j.jsames.2021.103322.

Aslanian, D. & Moulin, M. (2010). Comment on "A new scheme for the opening of the South Atlantic Ocean and the dissection of an Aptian salt basin" by Trond H. Torsvik, Sonia Rousse, Cinthia Labails and Mark A. Smethurst. *Geophysical Journal International*, 183, pp.20–28. DOI:10.1111/j.1365-246X.2010.04727.x.

Aslanian, D. & Moulin, M. (2012). Palaeogeographic consequences of conservational models in the South Atlantic Ocean. *Geological Society, London, Special Publications*, 369, pp.75–90. DOI:10.1144/SP369.5.

Aslanian, D., Moulin, M., Olivet, J.-L., Unternehr, P., Matias, L., Bache, F., Rabineau, M., Nouzé, H., Klingelhöfer, F. & Contrucci, I. (2009). Brazilian and African passive margins of the Central Segment of the South Atlantic Ocean: Kinematic constraints. *Tectonophysics*, 468, pp.98–112. DOI:10.1016/J.TECTO.2008.12.016.

Assumpção, M., Bianchi, M., Julià, J., Dias, F.L., França, G.S., Nascimento, R., Drouet, S., Pavão, César Garcia, Albuquerque, D.F. & Lopes, A.E. (2013). Crustal thickness map of Brazil: data compilation and main features. *Journal of South American Earth Sciences*, 43, pp.74–85. DOI:10.1016/j.jsames.2012.12.009.

van Avendonk, H.J.A, Holbrook, W.S., Nunes, G.T., Shillington, D.J., Tucholke, B.E., Louden, K.E., Larsen, H.C. & Hopper, J.R. (2006). Seismic velocity structure of the rifted margin of the eastern Grand Banks of Newfoundland, Canada. *Journal of Geophysical Research: Solid Earth*, 111. DOI:10.1029/2005JB004156.

Bécel, A., Davis, J.K., Shuck, B.D., Avendonk, V. & Gibson, J.C. (2020). Evidence for a prolonged continental breakup resulting from slow extension rates at the eastern north american volcanic rifted margin. *Journal of Geophysical Research: Solid Earth*, 125. DOI:10.1029/2020jb020093.

Bezerra, F.H.R., Nascimento, A.F., Ferreira, J.M, Nogueira, F.C., Fuck, R., Brito Neves, B.B., & Sousa, M.O.L. (2011). Review of active faults in the Borborema Province, Intraplate South America — Integration of seismological and paleoseismo-logical data. *Tectonophysics* 510.3-4, pp. 269–290. DOI: 10.1016/j.tecto.2011.08.005.

Bizzi, L.A., Schobbenhaus, C., Vidotti, R.M. & Gonçalves, J.H. eds., (2003). *Geologia, tectônica e recursos minerais do Brasil : texto, mapas & SIG*. CPRM – Serviço Geológico do Brasil. ISBN: 85-230-0790-3.

Blaich, O.A., Faleide, J.I., Tsikalas, F., Lilletveit, R., Chiossi, D., Brockbank, P. & Cobbold, P. (2010). Structural architecture and nature of the continent-ocean transitional domain at the Camamú and Almada Basins (NE Brazil) within a conjugate margin setting. In: *Geological society of London*. pp.867–883. DOI:10.1144/0070867.

Blaich, O.A., Tsikalas, F. & Faleide, J.I. (2008). Northeastern Brazilian margin: Regional tectonic evolution based on integrated analysis of seismic reflection and potential field data and modelling. *Tectonophysics*, 458, pp.51–67. DOI:10.1016/J.TECTO.2008.02.011.

Boillot, G., Recq, M., L, W.E., W, M.A., Applegate, J., Baltuck, M., A, B.J., C, C.M., A, D.T., Dunham, K. et al. (1987). Tectonic denudation of the upper mantle along passive margins: a model based on drilling results (ODP leg 103, western Galicia margin, Spain). *Tectonophysics*, 132, pp.335–342. DOI:10.1016/0040-1951(87)90352-0.

Bonifacio, J.F., Ganade, C.E., dos Santos, A.C. & Ferreira da Trindade, R.I. (2023). Review and critical assessment on plate reconstruction models for the South Atlantic, Earth-Science Reviews 238, 104333. DOI:/10.1016/j.earscirev.2023.104333.

Bott, (1971). Evolution of young continental margins and formation of shelf basins. *Tectonophysics*, 11, pp.319–327. DOI:10.1016/0040-1951(71)90024-2.

Buck, W.R., Lavier, L.L. & Poliakov, A.N.B. (1999). How to make a rift wide. *Philosophical Transactions-Royal Society of London Series a Mathematical Physical and Engineering Sciences*, pp. 671–689. DOI: 10.1098/rsta.1999.0348.

Bullock, A.D. & Minshull, T.A. (2005). From continental extension to seafloor spreading: crustal structure of the Goban Spur rifted margin, southwest of the UK. *Geophysical Journal International*, 163, pp.527–546. DOI:10.1111/j.1365-246x.2005.02726.x.

Caixeta, José Maurício, Ferreira, T.S., Machado, Teixeira, J.L. & Marco (2015). Albian rift systems in the northeastern brazilian margin: An example of rifting in hyper-extended continental crust. *AAPG ICE 2014*, DOI:10.13140/RG.2.1.3300.9769.

Caixeta, J.M., Silva, W., R.E., Sérgio, I. & Gontijo, G.A. (2007). Bacias de Camamú. *Boletim de Geociências da Petrobrás*, 15, pp.455–461.

Chaboureau, A.-C., Guillocheau, F., Robin, C., Rohais, S., Moulin, M. & Aslanian, D. (2013). Paleogeographic evolution of the central segment of the South Atlantic during Early Cretaceous times: Paleotopographic and geodynamic implications. *Tectonophysics*, 604, pp.191–223. DOI:10.1016/j.tecto.2012.08.025.

Chauvet, F., Sapin, F., Geoffroy, L., Ringenbach, J. C., & Ferry, J. N. (2021). Conjugate volcanic passive margins in the austral segment of the South Atlantic–Architecture and development. *Earth-Science Reviews*, *212*, 103461. DOI:10.1016/j.earscirev.2020.103461

Chian, D., Louden, K.E., Minshull, T.A. & Whitmarsh, R.B. (1999). Deep structure of the ocean-continent transition in the southern Iberia Abyssal Plain from seismic refraction profiles: Ocean Drilling Program (Legs 149 and 173) transect. *Journal of Geophysical Research: Solid Earth*, 104, pp.7443–7462. DOI:10.1029/1999jb900004.

Christensen, N. & Mooney, W. (1995). Seismic velocity structure and composition of the continental crust: A global view. *Journal of Geophysical Research Atmospheres*, 100, pp.9761–9788. DOI:10.1029/95JB00259.

Christeson, G.L., Goff, J.A. & Reece, R.S. (2019). Synthesis of oceanic crustal structure from two-dimensional seismic profiles. *Reviews of Geophysics*, 57, pp.504–529. DOI:10.1029/2019rg000641.

Clerc, C., Jolivet, L. & Ringenbach, J.-C. (2015). Ductile extensional shear zones in the lower crust of a passive margin. *Earth and Planetary Science Letters*, 431, pp.1–7. DOI:10.1016/j.epsl.2015.08.038.

Cohen, J. K. & J. W. Stockwell Jr., eds. (2015). CWP/SU: Seismic Un*x Release No. 44R1: an open source software package for seismic research and processing.

Contrucci, I., Matias, L., Moulin, M., Géli, L., Klingelhoefer, F., Nouzé, H., Aslanian, D., Olivet, J.L., Réhault, J-P. & Sibuet, J-C. (2004). Deep structure of the West African continental margin (Congo, Zaïre, Angola), between 5 S and 8 S, from reflection/refraction seismics and gravity data. *Geophysical Journal International* 158.2, pp. 529–553. doi: 10.1111/j.1365-246X.2004.02303.x.

Cook, F.A., White, D.J., Jones, A.G., David, Hall, J. & Clowes, R.M. (2010). How the crust meets the mantle: Lithoprobe perspectives on the Mohorovičić discontinuity and crust–mantle transition. *Canadian Journal of Earth Sciences*, 47, pp.315–351. DOI:10.1139/E09-076.

Dean, S. M., T. A. Minshull, R. B. Whitmarsh, & K. E. Louden (2000). Deep structure of the ocean-continent transition in the southern Iberia Abyssal Plain from seismic refraction profiles: The IAM-9 transect at 40 o 20N. *Journal of Geophysical Research: Solid Earth* 105.B3, pp. 5859–5885. ISSN: 0148-0227. DOI: 10.1029/1999jb900301.

Delgado, I.M., Souza, J.D., Silva, L.C., Silveira Filho, N.C., Santos, R.A., Pedreira, A.J., Guimarães, J. T., Angelim, L.A.Q., Vasconcelos, A.M., Gomes, I.P., Lacerda Filho, J.V., Valente, C.R., Perrota, M.M. & Heineck, C.A. (2003). *Geotectônica do escudo atlântico. Geologia, tectônica e recursos minerais do Brasil : texto, mapas & SIG* Ed by Bizzi, L.A., Schobbenhaus, C., Vidotti,R.M. & Gonçalves, J.H. CPRM – Serviço Geológico do Brasil, chap V, pp.227–334.

Dias, T.G., de, F., Pedrosa-Soares, Antônio Carlos, Stevenson, R., Dussin, I., Luiz, S., Alkmim, F. & Pimentel, M. (2016). Age, provenance and tectonic setting of the high-grade Jequitinhonha Complex, Araçuaí Orogen, eastern Brazil. *Brazilian Journal of Geology*, 46, pp.199–219. DOI:10.1590/2317-4889201620160012.

Dominguez, José Maria Landim, Rian Pereira da Silva, Alina Sá Nunes, and Antônio Fernando Menezes Freire (2013). "The narrow, shallow, low-accommodation shelf of central Brazil: Sedimentology, evolution, and human uses". In: Geomorphology 203, pp. 46–59. ISSN : 0169-555X. DOI :10.1016/j.geomorph.2013.07.004.

Dupré, S., Cloetingh, S. and Bertotti, G. (2011). Structure of the Gabon Margin from integrated seismic reflection and gravity data. *Tectonophysics*, 506, pp.31–45. DOI:10.1016/j.tecto.2011.04.009.

Eduardo, Vinicius, M., Fuck, Reinhardt A and Berrocal, J. (n.d.). Características sísmicas da litosfera da Província Borborema: resultados parciais do experimento de refração sísmica profunda. In: *European Association of Geoscientists & Engineers*. p.197.

Evain, M., Afilhado, A., Rigoti, C., Loureiro, A., Alves, D., Klingelhöfer, F., Schnürle, P., Feld, A., Fuck, R., Soares, J., Marcus, Corela, C., Matias, L., Benabdellouahed, M., Baltzer, A., Rabineau, M., Viana, A., Moulin, M. and Aslanian, D. (2015). Deep structure of the Santos Basin – São Paulo Plateau System, SE Brazil. *Journal of Geophysical Research*. DOI:10.1002/2014JB011561.

Evain, M. et al. (this issue). Along-strike segmentation of the northeastern Brazilian margins: geodynamic control and role of lithospheric inheritance. *Journal of South American Earth Sciences*

Ferreira, T.S. (2018). The Jequitinhonha-Almada-Camamu rift system: an approach to the rifting evolution on the northeast Brazilian margin. *Boletim de Geociências da Petrobrás* 23.1

Ferreira, T.S., Caixeta, José Maurício & Lima, D. (2009). Controle do embasamento no rifteamento das bacias de Camamú e Almada. *Boletim de Geociências da Petrobrás,* 17, pp.69–88.

Funck, T., Hopper, J.R., Larsen, H.C., Louden, K.E., Tucholke, B.E. & Steven, H.W. (2003). Crustal structure of the ocean-continent transition at Flemish Cap: Seismic refraction results. *Journal of Geophysical Research: Solid Earth*, 108. DOI:10.1029/2003JB002434.

Gontijo, G.A., Milhomem, PdS, Caixeta, J.M., Dupuy, ISS & Menezes, PEL (2007). "Bacia de Almada". In: Boletim de Geociˆencias da PETROBRAS 15.2, pp. 463–473.

Guan, H., Geoffroy, L., Gernigon, L., Chauvet, F., Grigné, C., & Werner, P. (2019). Magmatic ocean-continent transitions. *Marine and Petroleum Geology*, *104*, 438-450. DOI:10.1016/j.marpetgeo.2019.04.003

Halla, M.M.S., Dominguez, J.M.L & Corrêa-Gomes,L.C. (2019). Structural controls on the morphology of an extremely narrow, low-accommodation, passive margin shelf (Eastern Brazil). *Geo-Marine Letters* 40.6, pp. 865–878. DOI: 10.1007/s00367-019-00605-y.

Hammer, P. T. C. and R. M. Clowes (1997). Moho reflectivity patterns – a comparison of Canadian lithoprobe transects. *Tectonophysics*, 269, pp.179–198. DOI:10.1016/S0040-1951(96)00164-3.

Hardie, L.A. (1990). The roles of rifting and hydrothermal CaCl 2 brines in the origin of potash evaporites; an hypothesis. *American Journal of Science*, 290, pp.43–106. DOI:10.2475/ajs.290.1.43.

Hasui, Y., Carneiro, C.D.R., Almeida, F.F.M. & Bartorelli, A. eds., (2012). *Geologia do Brasil*. Beca. ISBN: 9788562768101.

Havskov, J. & Ottemöller, L. (1999). SEISAN earthquake analysis software. *Seismol. Res. Lett.*, 70, pp.532–534.

Heine, C., Zoethout, J. & Dietmar, M.R. (2013). Kinematics of the South Atlantic rift. *Solid Earth*. DOI:10.5194/se-4-215-2013.

Holz, M., Vilas-Boas, D.B., Troccoli, E.B., Santana, V.C. & Vidigal-Souza, P.A. (2017). Conceptual models for sequence stratigraphy of continental rift successions. *Advances in Sequence Stratigraphy*, pp.119–186. DOI:10.1016/bs.sats.2017.07.002.

IHO-IOC GEBCO (2014). *The GEBCO 2014 grid, version 20150318*. Last access: 2017-01-20

Klingelhöfer, F., Evain, M., Afilhado, A., Rigoti, C., Loureiro, A., Alves, D., Leprêtre, A., Moulin, M., Schnürle, P., Benabdellouahed, M., Baltzer, A., Rabineau, M., Feld, A., Viana, A. & Aslanian,

D. (2015). Imaging proto-oceanic crust off the Brazilian Continental Margin. *Geophysical Journal International*, 200(1), pp.471–488. DOI:10.1093/GJI/GGU387.

Küchle, J., Holz, M., Brito, A.F. & Bedregal, R.P. (2005). Análise estratigráfica de bacias rifte: aplicação de conceitos genéticos nas bacias de Camamu-Almada e Jequitinhonha. *Boletim de Geociências da Petrobrás*, 13, pp.227–244.

Lima, M.V.A.G., Berrocal, J., Soares, J.E.P. & Fuck, R.A. (2015). Deep seismic refraction experiment in northeast Brazil: New constraints for Borborema province evolution. *Journal of South American Earth Sciences* 58, pp. 335–349. DOI: 10.1016/j.jsames.2014.10.007.

Liu, Z. & Bleistein, N. (1995). Migration velocity analysis: Theory and an iterative algorithm. *Geophysics*, 60, pp.142–153. DOI:10.1190/1.1443741.

Lopes, L.R. (2017). *Modelagem da estrutura crustal sob a porção sul do perfil NS da província Borborema e cráton São Francisco: um estudo de refração sísmica profunda*. Universidade Federal do Pampa. PhD thesis.

Loureiro, A., Afilhado, A., Matias, L., Moulin, M. & Aslanian, D. (2016). Monte Carlo approach to assess the uncertainty of wide-angle layered models: Application to the Santos Basin, Brazil. *Tectonophysics*, 683, pp.286–307. DOI:10.1016/j.tecto.2016.05.040.

Loureiro, A., Schnürle, P., Klingelhoefer, F., Afilhado, A., Evain, M., Gallais, F., Rabineau, M., Baltzer, A., Benabdellouahed, M., Pinheiro, J.M., Dias, N., Soares, J., Fuck, R., Cupertino, J.A., Viana, A.R., Matias, L., Moulin, M., Aslanian, D. & the SALSA team (2018). Imaging exhumed lower continental crust in the distal Jequitinhonha basin, Brazil. *Journal of South American Earth Sciences*, 84, pp.351–372. DOI:10.1016/j.jsames.2018.01.009.

Ludwig, W.J., Nafe, J.E. and Drake, C.L. (1970). Seismic refraction. *The sea*, 4, pp.53–84.

Manatschal, G., Froitzheim, N., Rubenach, M. & Turrin, D.B. (2001). The role of detachment faulting in the formation of an ocean-continent transition: insights from the Iberia Abyssal Plain. *Geological Society, London, Special Publications*, 187, pp.405–428. DOI:10.1144/gsl.sp.2001.187.01.20.

Menezes, P. E. d. L. & P. d. S. Milhomem (2009). Tectônica de sal nas bacias de Cumuruxatiba, do Almada e de Camamu. *Sal: geologia e tectônica*. Ed. by W. U. Mohriak, P. Szatmari, & S. M. Couto Anjos. Sao Paulo: Editora Beca. Chap. XI, pp. 253–273.

Mével, C. (2003). Serpentinization of abyssal peridotites at mid-ocean ridges. *Comptes Rendus Geoscience*, 335, pp.825–852. DOI:10.1016/j.crte.2003.08.006.

Minshull, T.A. (2009). Geophysical characterisation of the ocean–continent transition at magma-poor rifted margins. *Comptes Rendus Geoscience*, 341, pp.382–393. DOI:10.1016/j.crte.2008.09.003.

Mohriak, Webster Ueipass (2003). Bacias sedimentares da margem continental brasileira. CPRM – Serviço Geológico do Brasil, pp.87–165.

Moulin, M., Aslanian, D., Olivet, J.-L., Contrucci, I., Matias, L., Géli, L., Klingelhöfer, F., Nouzé, H., Réhault, J.-P. & Unternehr, P. (2005). Geological constraints on the evolution of the Angolan margin based on reflection and refraction seismic data (ZaïAngo project). *Geophysical Journal International*, 162, pp.793–810. DOI:10.1111/j.1365-246X.2005.02668.x.

Moulin, M., Aslanian, D. & Unternehr, P. (2010). A new starting point for the South and Equatorial Atlantic Ocean. *Earth-Science Reviews*, 98, pp.1–37. DOI:10.1016/j.earscirev.2009.08.001.

Moulin, M., Klingelhöfer, F., Afilhado, A., Aslanian, D., Schnürle, P., Nouzé, H., Rabineau, M., Beslier, M.-O. & Feld, A. (2015). Deep crustal structure across a young passive margin from wide-angle and reflection seismic data (The SARDINIA Experiment) – I. Gulf of Lion's margin. *Bulletin de la Société Géologique de France*, 186, pp.309–330. DOI:10.2113/gssgfbull.186.4-5.309.

Moulin, M., Philippe Schnurle, Afilhado, A., Gallais, F., Dias, N., Mikael Evain, Soares, J., Reinhardt Fuck, Pessoa, C., Viana, A. & Aslanian, D. (2021). Imaging early oceanic crust spreading in the equatorial atlantic ocean: Insights from the MAGIC wide-angle experiment. *Journal of South American Earth Sciences*, 111, p.103493. DOI:10.1016/j.jsames.2021.103493.

Müller, R.D. Seton, M., Zahirovic, S., Williams, S.E., Matthews, K.J., Wright, N.M., Shephard, G.E., Maloney, K.T., Barnett-Moore, N., Maral Hosseinpour, Bower, D.J. & Cannon, J. (2016). Ocean basin evolution and global-scale plate reorganization events since pangea breakup. *Annual Review of Earth and Planetary Sciences*, 44, pp.107–138. DOI:10.1146/annurev-earth-060115-012211.

Mutter, C.Z. & Mutter, J.C. (1993). Variations in thickness of layer 3 dominate oceanic crustal structure. *Earth and Planetary Science Letters*, 117, pp.295–317. DOI:10.1016/0012-821x(93)90134-u.

Pinheiro, J.M., P. Schnurle, M. Evain, A. Afilhado, F. Gallais, Klingelhoefer, F., Loureiro, A., R. Fuck, Soares, J., Cupertino, J.A., Viana, A., M. Rabineau, Baltzer, A., M. Benabdellouahed, Dias, N., Moulin, M., Aslanian, D., Morvan, L., J.P. Mazé & Pierre, D. (2018). Lithospheric structuration onshore-offshore of the Sergipe-Alagoas passive margin, NE Brazil, based on wide-angle seismic data. *Journal of South American Earth Sciences*. DOI:10.1016/j.jsames.2018.09.015.

Porada, H. (1989). Pan-African rifting and orogenesis in southern to equatorial Africa and eastern Brazil. *Precambrian Research*, 44, pp.103–136. DOI:10.1016/0301-9268(89)90078-8.

Poudjom Djomani, Y.H., O'Reilly, S.Y., Griffin, W.L. & Morgan, P. (2001). The density structure of subcontinental lithosphere through time. *Earth and Planetary Science Letters* 184.3-4, pp. 605–621. ISSN: 0012-821X. DOI: 10.1016/s0012-821x(00)00362-9.

Prodehl, C., Kennett, B., Artemieva, I.M. & Thybo, H. (2013). 100 years of seismic research on the Moho. *Tectonophysics*, 609, pp.9–44. DOI:10.1016/j.tecto.2013.05.036.

Rangel, H.D., de Oliveira, J.L.F. & Caixeta, J.M. (2007). Bacia de Jequitinhonha. *Boletim de Geociências da PETROBRAS 15*, pp. 475–483.

Romito, S. and Mann, P. (2022). Crustal structure of the camamu-almada margin along the northeastern rift segment of brazil from an integration of deep-penetration seismic reflection profiles, refraction, and gravity modeling. *Tectonics*, 41. DOI:10.1029/2021tc007157.

Rosendhal, B.R., Groschel-Becker, H., Meyers, J. & Kaczmarick, K. (1991). Deep seismic reflection study of a passive margin, southeastern Gulf of Guinea. *Geology*, 19, pp.291–295. DOI:2.3.co;2">10.1130/0091-7613(1991)019<0291:dsrsoa>2.3.co;2.

Sandwell, D.T., Dietmar, M.R., Walter, Garcia, E. & Francis, R. (2014). New global marine gravity model from CryoSat-2 and Jason-1 reveals buried tectonic structure. *Science*, 346, pp.65–67. DOI:10.1126/science.1258213.

Sandwell, D.T., Garcia, E., Soofi, K., Wessel, P., Chandler, M. & Smith, W.F. (2013). Toward 1-mGal accuracy in global marine gravity from CryoSat-2, Envisat, and Jason-1. *The Leading Edge*, 32, pp.892–899. DOI:10.1190/tle32080892.1.

Sandwell, D.T. & Smith, W.F. (2009). Global marine gravity from retracked Geosat and ERS-1 altimetry: Ridge segmentation versus spreading rate. *Journal of Geophysical Research*, 114. DOI:10.1029/2008jb006008.

Schobbenhaus, C. & deBrito Neves, B.B. (2003). A geologia do brasil no contexto da plataforma sul-americana. In: Bizzi, Luiz Augusto, C. Schobbenhaus, R.M. Vidotti and Gonçalves, João Henrique, eds. CPRM – Serviço Geológico do Brasil, pp.5–54.

Scotchman, I. and Chiossi, D. (2008). Kilometre-scale uplift of the Early Cretaceous rift section, Camamú basin, offshore North-East Brazil.*Talk presented at AAPG International Conference and Exhibition, Cape Town.*

Shuck, B. D., van Avendonk, H. J., & Bécel, A. (2019). The role of mantle melts in the transition from rifting to seafloor spreading offshore eastern North America. *Earth and Planetary Science Letters*, *525*, 115756. DOI:10.1016/j.epsl.2019.115756

Sibuet, J.C. Rouzo, S. & Srivastava, S. (2012). Plate tectonic reconstructions and paleogeographic maps of the central and North Atlantic oceans. *Canadian Journal of Earth Sciences*, 49, pp.1395–1415. DOI:10.1139/e2012-071.

Soares, J.E.P., Lima, M.V. Fuck, R.A. & Berrocal, J. (2010). Características sísmicas da litosfera da Província Borborema: resultados parciais do experimento de refração sísmica profunda. *IV Simpóosio Brasileiro de Geofísica. European Association of Geoscientists & Engineers*, p. 197.

Souza, J.D., Kosin, M., Teixeira, L.R., Martins, A.A.M., Bento, R.V., Borges, V.P., Leite, C.A. & Arcanjo, J.B. (2004). Carta geológica do Brasil ao milionésimo - Folha Salvador SD-24. *Sistema de Informações Geográficas - SIG, Programa Geologia do Brasil. CPRM* Ed. by Schobbenhaus, C., Gonçalves, J.H. , Santos, J.O.S., Abram, M.B., Neto, L., Matos, G.M.M., Vidotti, R.M., Ramos, M.A.B., & de Jesus, J.D.A. Brasília.

Stockwell, J.W. (1999). The CWP/SU: Seismic Un*x package,. *Computers & Geosciences*, 25, pp.415–419. DOI:10.1016/s0098-3004(98)00145-9.

Tavares, E.J., Eduardo, Fuck, R.A. & Vicinius, M. (2012). Modelagem de onda p e razão Vp/Vs da crosta sob a linha de refração sísmica profunda NW-SE da província Borborema. *IV Simpóosio Brasileiro de Geofísica. European Association of Geoscientists & Engineers*. p.341.

Torsvik, Trond H, Rousse, S., Labails, C. and Smethurst, M.A. (2009). A new scheme for the opening of the South Atlantic Ocean and the dissection of an Aptian salt basin. *Geophysical Journal International*, 177, pp.1315–1333. DOI:10.1111/j.1365-246X.2009.04137.x.

Tozer, B., Sandwell, D.T., Smith, W.H., Olson, C., Beale, J. & Wessel, P. (2019). Global bathymetry and topography at 15 arc sec: SRTM15+. *Earth and Space Science*, 6, pp.1847–1864.

Trompette, R. (1997). Neoproterozoic (~600 ma) aggregation of western gondwana: a tentative scenario. *Precambrian Research*, 82, pp.101–112. DOI:10.1016/S0301-9268(96)00045-9.

Vales, D., Dias, N.A., Rio, I., Matias, L., Silveira, G., Madeira, J., Weber, M., Carrilho, F. & Haberland, C. (2014). Intraplate seismicity across the Cape Verde swell: A contribution from a temporary seismic network. *Tectonophysics*, 636, pp.325–337. DOI:10.1016/j.tecto.2014.09.014.

Wessel, P. and Müller, R. (2016). *The global seafloor fabric and magnetic lineation data base*. [online] Available at: http://www.soest.hawaii.edu/PT/GSFML/.

Wessel, P. & Smith, W.H.F. (1996). A global, self-consistent, hierarchical, high-resolution shoreline. *Journal of Geophysical Research*, 101, pp.8741–8743. DOI:10.1029/96JB00104.

Wessel, P. & Smith, W.H.F. (1998). New, improved version of Generic Mapping Tools released. *Eos, Transactions American Geophysical Union*, 79, pp.579–579. DOI:10.1029/98EO00426.

White, R.S. (1992). Crustal structure and magmatism of North Atlantic continental margins. *Journal of the Geological Society*, 149, pp.841–854. DOI:10.1144/gsjgs.149.5.0841.

White, R.S., McKenzie, D. & Keith, O.R. (1992). Oceanic crustal thickness from seismic measurements and rare earth element inversions. *Journal of Geophysical Research: Solid Earth (1978–2012)*, 97, pp.19683–19715. DOI:10.1029/92JB01749.

Whitmarsh, R.B., White, R.S., Horsefield, S.J., Sibuet, J.-C., Recq, M. & Louvel, V. (1996). The ocean-continent boundary off the western continental margin of Iberia: Crustal structure west of Galicia Bank. *Journal of Geophysical Research: Solid Earth*, 101, pp.28291–28314. DOI:10.1029/96JB02579.

Zelt, C.A. (1999). Modelling strategies and model assessment for wide-angle seismic traveltime data. *Geophysical Journal International*, 139, pp.183–204. DOI:10.1046/J.1365-246X.1999.00934.X.

Zelt, C.A. & Smith, R.B. (1992). Seismic traveltime inversion for 2-D crustal velocity structure. *Geophysical Journal International*, 108, pp.16–34. DOI:10.1111/J.1365-246X.1992.TB00836.X.

TABLES

Table 1: Statistics for the data fit of the velocity model of profile SL09.

Table 2: Gravity modelling of profile SL09. Densities converted from seismic propagation velocities for SL09, according to Ludwig et al. (1970) and gravity modelling results.

Table S3 (supplemental): 1D model used for hypocentral determination.

FIGURES

Figure 1: Location of profiles of the SALSA mission. a) satellite-derived gravimetric anomaly in the sea (Sandwell & Smith 2009; Sandwell et al. 2013; Sandwell et al. 2014) and topography on land (IHO-IOC GEBCO 2014). Circles denote OBS deployments. Triangles denote land stations. Black solid lines indicate MCS sections. Yellow star indicates approximate location of the earthquake used for modelling. Dashed black line denotes faults. Dashed white lines indicate marine basin limits (Bizzi et al. 2003). Dashed red lines indicate the extent of the Jequitinhonha-Almada-Camamu (JAC) rift system. Orange area indicates the Recôncavo-Tucano-Jatobá (RTJ) basins (Bizzi et al. 2003). Light blue area indicates the limits of the São Francisco Craton, adapted from (Hasui et al. 2012). TMAZ: Taipus-Mirim Accommodation Zone. Main rivers indicated by solid blue lines (Wessel & Smith 1996). Yellow lines indicate position of the A and B GXT profiles used in the interpretation by (Romito & Mann 2022). b) General location map of studied area and conjugate margin highlighted with red rectangles. STRM15+ bathymetry (Tozer et al. 2019). Orange lines indicate fracture zone tracks (Wessel & Müller 2016). c) Location of the Barra and Itapuã faults, adapted from (Halla et al. 2019).

Figure 2: MCS record section for SALSA09. Solid coloured lines indicate the modelled interfaces. White triangles denote OBS locations. Dark blue vertical line indicates crossing with SL06. HV – High Velocity zone.

Figure 3: Instrument SL09OBS16. a) Record section. b) Synthetic record section. c) Synthetic record section, coloured according to their identified arrivals. d) Picked arrivals coloured according to interfaces and type of arrival, their error bars, and solid black lines indicating the predicted arrival times. e) Ray tracing over the model. f) Comparison with the MCS section, coloured lines match the reflected arrivals colours from d) and colour scale from Fig. 2. All time sections reduced to 7 km/s.

Figure 4: Instrument SL09OBS08. aa) Record section. b) Synthetic record section. c) Synthetic record section, coloured according to their identified arrivals. d) Picked arrivals coloured according to interfaces and type of arrival, their error bars, and solid black lines indicating the predicted arrival times. e) Ray tracing over the model. f) Comparison with the MCS section, coloured lines match the reflected arrivals colours from d) and colour scale from Fig. 2. All time sections reduced to 7 km/s.

Figure 5: Instrument SL09OBS04. a) Record section. b) Synthetic record section. c) Synthetic record section, coloured according to their identified arrivals. d) Picked arrivals coloured according to interfaces and type of arrival, their error bars, and solid black lines indicating the predicted arrival times. e) Ray tracing over the model. f) Comparison with the MCS section, coloured lines match the reflected arrivals colours from d) and colour scale from Fig. 2. All time sections reduced to 7 km/s.

Figure 6: Instrument SL09OBS11. a) Record section. b) Synthetic record section. c) Synthetic record section, coloured according to their identified arrivals. d) Picked arrivals coloured according to interfaces and type of arrival, their error bars, and solid black lines indicating the predicted arrival times. e) Ray tracing over the model. f) Comparison with the MCS section, coloured lines match the reflected arrivals colours from d) and colour scale from Fig. 2. All time sections reduced to 7 km/s.

Figure 7: Instrument SL09OBS13. a) Record section. b) Synthetic record section. c) Synthetic record section, coloured according to their identified arrivals. d) Picked arrivals coloured according to interfaces and type of arrival, their error bars, and solid black lines indicating the predicted arrival times. e) Ray tracing over the model. f) Comparison with the MCS section, coloured lines match the reflected arrivals colours from d) and colour scale from Fig. 2. All time sections reduced to 7 km/s.

Figure 8: Instrument SL09LSS04. a) Record section. b) Synthetic record section. c) Synthetic record section, coloured according to their identified arrivals. d) Picked arrivals coloured according to interfaces and type of arrival, their error bars, and solid black lines indicating the predicted arrival times. e) Ray tracing over the model. f) Comparison with the MCS section, coloured lines match the reflected arrivals colours from d) and colour scale from Fig. 2. All time sections reduced to 7 km/s.

Figure 9: Instrument SL09LSS09. a) Record section. b) Synthetic record section. c) Synthetic record section, coloured according to their identified arrivals. d) Picked arrivals coloured according to interfaces and type of arrival, their error bars, and solid black lines indicating the predicted arrival times. e) Ray tracing over the model. f) Comparison with the MCS section, coloured lines match the reflected arrivals colours from d) and colour scale from Fig. 2. All time sections reduced to 7 km/s.

Figure 10: Instrument SL09LSS19. a) Record section. b) Synthetic record section. c) Synthetic record section, coloured according to their identified arrivals. d) Picked arrivals coloured according to interfaces and type of arrival, their error bars, and solid black lines indicating the predicted arrival times. e) Ray tracing over the model. f) Comparison with the MCS section, coloured lines match the reflected arrivals colours from d) and colour scale from Fig. 2. All time sections reduced to 7 km/s.

Figure 11: Final velocity model for profile SL09. Thick blue lines indicate interfaces in the basement constrained by reflections. Thick red lines indicate interfaces in the sedimentary basin constrained by reflections. Shaded area indicates ray coverage. Black triangles denote position of land stations and OBS. The crust on the São Francisco craton is comprised of upper crust, middle crust and lower crust. The middle and lower crusts thin out under the Camamu basin. From the necking zone towards the distal basin, a High Velocity zone (HV) and three intra mantle reflectors are present under the upper crust. a) Complete model, up to a depth of 60 km. b) Zoom to highlight the crustal structure in the basins.

Figure 12: Gravity modelling for profile SL09. a) Density model for profile SL09. Pink region indicates salt. b) Modelled (solid black line), observed gravity anomaly along profiles parallel to SL09 (solid yellow lines), and observed gravity anomaly along profile SL09 (red circles). c) Calculated load anomaly. d) Observed magnetic anomaly.

Figure 13: Pre-Stack Depth Migration analysis for SALSA09. a) Pre-stack depth migrated MCS record section for SALSA09. b) RMO analysis of the pre-stack depth migrated MCS record section

of SALSA09. Solid coloured lines indicate the modelled interfaces. White triangles denote OBS locations. Red vertical line indicates crossing with profile SL06.

Figure 14: Four estimators of model quality for SL09. a) Parameterization of the velocity model. Thin black lines indicate interfaces and squares indicate depth nodes. Reflective segments of interfaces are highlighted in blue. All velocity and depth nodes in the basement were evaluated. The nodes defining the depth of sedimentary layers are not evaluated, since they are constrained by the MCS data. b) Hitcounts. Colour of squares indicates the hitcount for those depth nodes. c) Smearing. Colour of squares indicates the smearing for those depth nodes. d) Resolution. Gray and yellow areas are considered well resolved in terms of velocities. Squares indicated depth nodes in the basement, coloured according to their resolution.

Figure 15: Uncertainty estimation for SL09. a) and b): Model uncertainties for profile SL09 according to (Loureiro et al. 2016), built from 13 models within the same quality thresholds as the preferred SL09 model. Red/blue shades denote maximum admissible velocity increases/decreases from the preferred solution. Black lines denote modelled interfaces. Yellow bands indicate interface depth uncertainties resulting from the variation of the propagation velocity. c) Velocity-depth profiles with uncertainty bounds: velocity-depth range of 49968 random models (grey), velocity-depth range of 55 models with a score as least as good as the preferred model's (yellow) and velocity-depth range of 13 models within the thresholds of number of rays, χ^2 and time RMS residual of SL09 model (orange). SL09 model's and best random model's velocity-depth profiles are indicated by continuous black line and dashed white respectively.

Figure 16: Comparison with ION GXT-2100. Overlay of main units of SL09 model (thick coloured lines) to line-drawing of ION GXT-2100 (thin lines). Red question mark indicates reflectors not visible on the wide-angle data. HV – High Velocity zone.

Figure 17: Domain segmentation along SL09. a) Distribution of 1D velocity profiles taken at each 10 km from the final P-wave velocity model and colour-coded according to segmentation along profile SL09. Grey zone corresponds to Domain 2 from Romito and Mann (2022). Red arrow indicates layer U. HV – High Velocity zone. b), c), f), g) and h) 1D velocity-depth profiles taken below the seafloor. d), e), i), j) and k) 1D velocity-depth profiles taken below the basement.

Figure 18: Nature of layer U, with uncertainty bounds. a) to e) Velocity-depth profiles with uncertainty bounds below basement, excluding layer U (dark orange) and including layer U (light orange). Necking domain is given for reference and salt is coloured in pink. SL09 model's and best random model's velocity-depth profiles are indicated by the continuous black line and the dashed white line, respectively. f) and g) dispersion of velocity-depth profiles taken at 10 km intervals including (light orange) and excluding (dark orange) layer U in the Necking and Camamu domains. Green arrow highlights velocity inversion at the top of layer U.

Figure 19: Comparison with profiles SL01 and SL02. a) Comparison of P-wave velocity as a function of depth below basement for the unthinned crust in São Francisco craton (SL09 - purple lines, this study) and the unthinned crust in the Sergipano Fold Belt (SL02 - green lines, Pinheiro et al. (2018)); b) Comparison of P-wave velocity as a function of depth below basement for the Necking domains of SL09 (blue lines), SL01 (orange lines) and SL02 (red lines). Pink and blue regions indicated a compilation of continental crusts (Christensen & Mooney 1995).

Figure 20: Extension of the necking domain. Comparison between the extension of necking domains in the Camamu margin (SL09, this study) and the Sergipe-Alagoas margin (SL02, Pinheiro et al. (2018)). The crust thins abruptly in the Camamu margin when compared with the Sergipe-Alagoas margin.

Figure 21: Comparison with exhumed mantle and proto-oceanic crust domains. a), b), d) and e) P-wave velocity as a function of depth below basement for the Camamu, Almada and distal basins, compared with wide-angle seismic models where ocean-transition zones were interpreted as exhumed and/or serpentinized upper mantle (shaded areas). Lilac regions indicate velocity-depth profiles from IAM-9 in Iberia Abyssal Plain (Dean et al. 2000). Brown regions indicate profiles from profile SCREECH-2 in the Grand Banks margin, offshore Newfoundland (van Avendonk et al. 2006). Dark blue regions indicate profiles from profile CAM in the Southern Galician margin (Chian et al. 1999). Grey regions indicate mean velocity-depth variations with one standard deviation above and below the mean of SCREECH-1, SCREECH-2, SCREECH-3, WAM, ISE-1, CAM-144 and IAM-9 models from (Minshull 2009). c) and f) Same comparison, but with proto-oceanic crusts in the Sardinia profiles (green regions) in the Provençal Basin (Moulin et al. 2015) and in the Santos basin (orange regions) (Klingelhöfer et al. 2015).

Figure 22: Comparison with exhumed continental crust domains. P-wave velocity as a function of depth below basement for the a) and d) Camamu, b) and e) Almada and c) and f) distal basins. Blue regions indicate 1D velocity-depth profiles taken along a region of Exhumed Continental Crust in the Provençal basin and Gulf of Lion (Afilhado et al. (2015) Moulin et al. (2015)). Brown regions indicate 1D velocity-depth profiles taken along a region of Exhumed Lower Continental Crust in the Jequitinhonha basin (Loureiro et al. 2018). Green regions indicate 1D velocity-depth profiles taken along a region of Exhumed Middle-Lower Continental Crust in the Santos basin (Evain et al. 2015). Yellow regions indicate 1D velocity-depth profiles taken along a region of Exhumed and intruded Middle-Lower Continental Crust in the Santos basin (Evain et al. 2015) .

Figure 23: Comparison with oceanic crust domains. P-wave velocity as a function of depth below basement for the Camamu, Almada and distal basins, compared with wide-angle seismic models where oceanic crust is interpreted (shaded areas). Lilac regions indicate a compilation of 1D velocity-depth profiles for oceanic crusts in the Atlantic Ocean aged 59 Ma to 127 Ma and 142 ma and 170 Ma (White 1992) Grey regions, oceanic crusts up to 170 Ma (Christeson et al. 2019).

Figure 24: Proposed segmentation. Map of all results acquired during the SALSA experiment (Loureiro et al., 2018; Pinheiro et al., 2018; Aslanian et al., this issue; Evain et al., this issue; Schnurle et al., this issue; and this article) and the compilation done by Assumption et al. (2013) on land. The crustal thicknesses are illustrated with different colours along the profiles and in boxes onland. The necking zones of the margins is limited by two thick dashed black lines. The crustal interpretations of the wide-angle seismic data are showed with coloured areas.

Figure S25 (supplemental): Microseismicity detected by the SALSA land stations. Earthquakes and quarry blasts detected by analyzing the coherent signals (Vales et al. 2014) found in the spectrograms of the land stations between April 8th and April 14th and between May 5th and May 19th, 2014. Not all land stations were deployed simultaneously. The seismic array is represented blue triangles. The events location are represented by circles with radius proportional to the number of stations that contributed to the localizations. Circle colours represent the different ranges of hypocentral depths. Orange star indicates the earthquake used on the modelling of profile SL09.

Declaration of interests

☒The authors declare that they have no known competing financial interests or personal relationships that could have appeared to influence the work reported in this paper.

☐The authors declare the following financial interests/personal relationships which may be considered as potential competing interests:

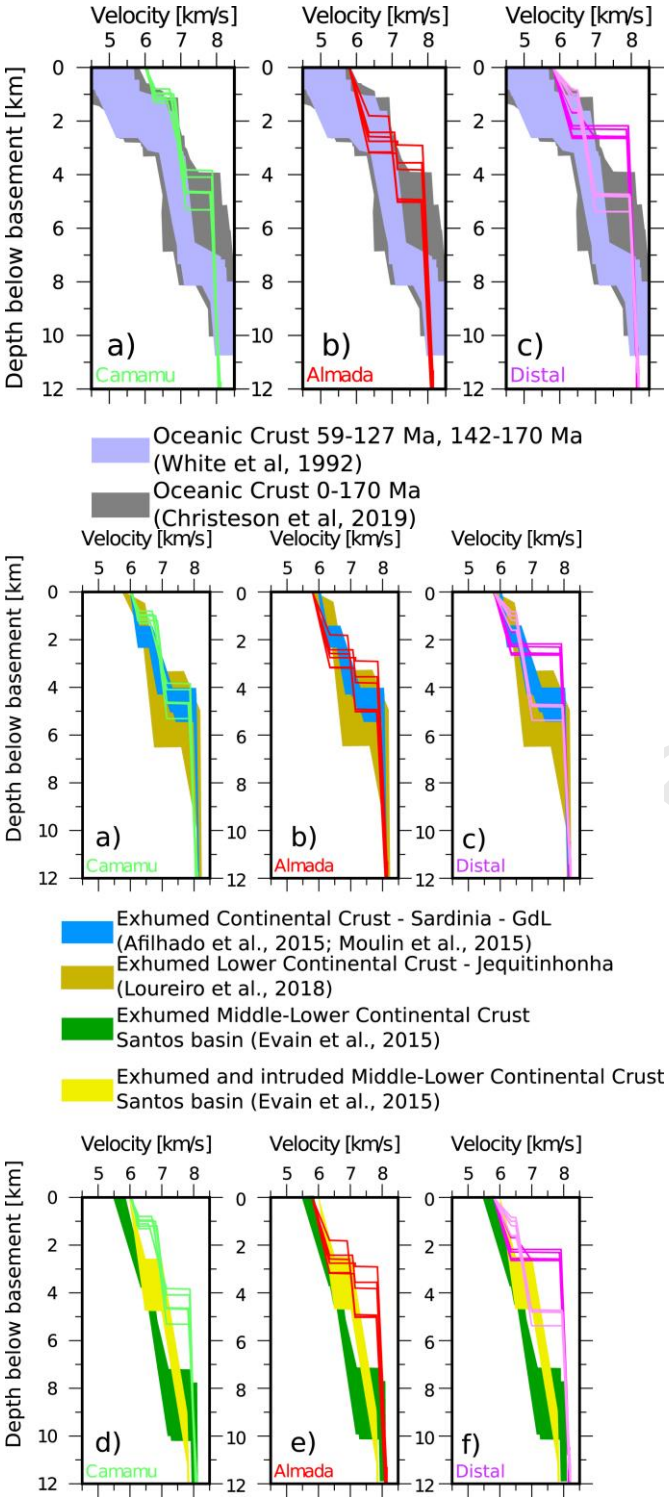
Velocity [km/s]
5 6 7 8
Depth below basement [km]
0 2 4 6 8 10 12
a)
Camamu
b)
Almada
c)
Distal
Oceanic Crust 59-127 Ma, 142-170 Ma
(White et al, 1992)
Oceanic Crust 0-170 Ma
(Christeson et al, 2019)
Exhumed Continental Crust - Sardinia - GdL
(Afilhado et al., 2015; Moulin et al., 2015)
Exhumed Lower Continental Crust - Jequitinhonha
(Loureiro et al., 2018)
Exhumed Middle-Lower Continental Crust
Santos basin (Evain et al., 2015)
Exhumed and intruded Middle-Lower Continental Crust
Santos basin (Evain et al., 2015)
d)
e)
f)

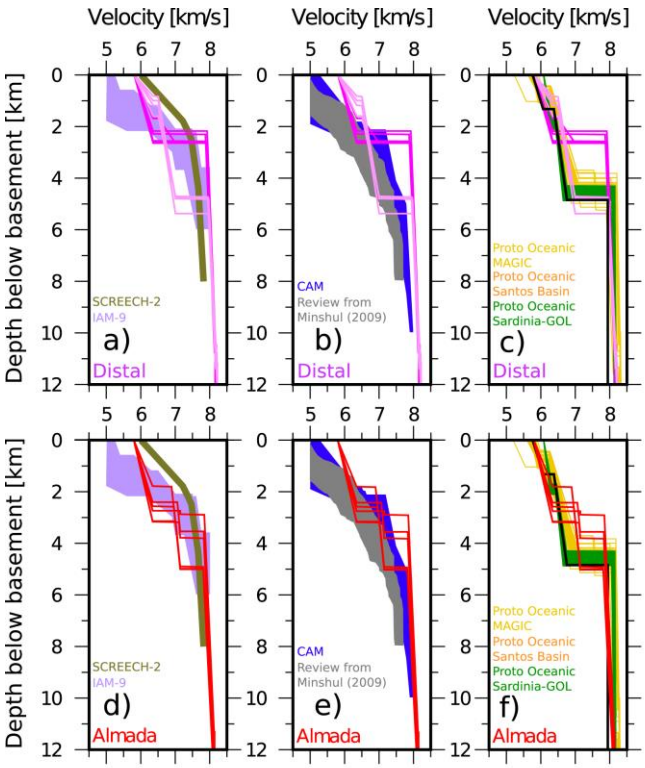

IAM-9 (Dean et al., 2000)

SCREECH-2 (van Avendonk et al.,2006)

CAM (Minshull et al., 1998; Chian et al., 1999)

Review from Minshull (2009)

Proto-oceanic - Santos basin (Klingelhöfer et al., 2015)

Proto-oceanic - Gulf of Lion (Moulin et al., 2015)

Proto-oceanic - MAGIC (Moulin et al., 2021)

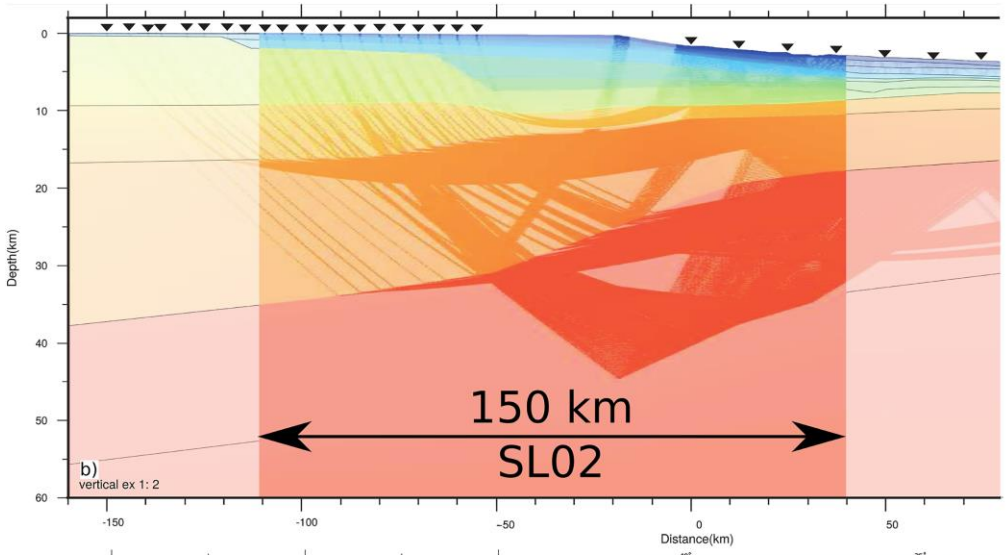
150 km
SL02
b)
vertical ex 1: 2
Depth(km)
Distance(km)

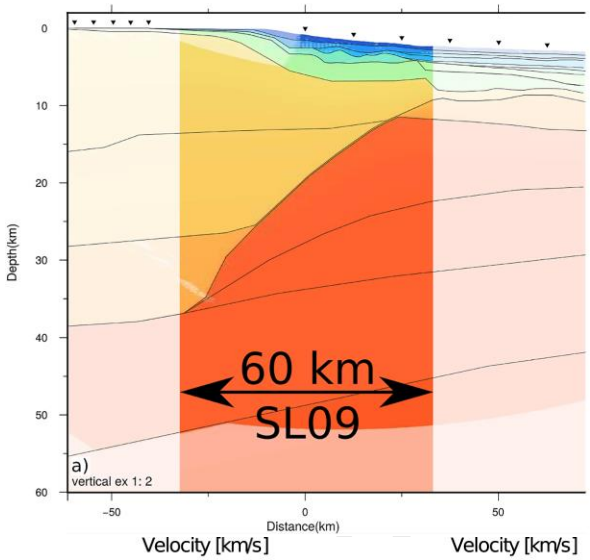
60 km
SL09
a)
vertical ex 1: 2
Depth(km)
Distance(km)

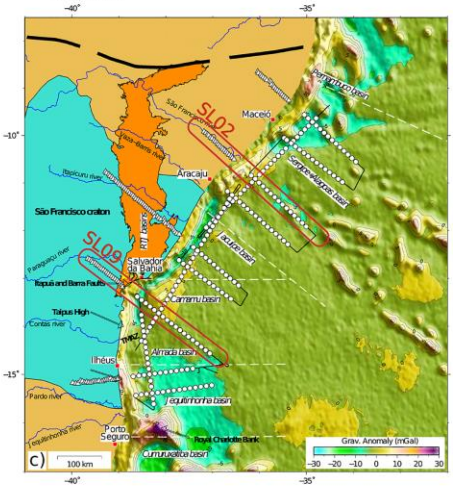
SL02
SL09
Maceió
Aracaju
São Francisco craton
Salvador da Bahia
Ilhéus
Porto Seguro
Jacuípe basin
Camamu basin
Almada basin
Jequitinhonha basin
Cumuruxatiba basin
Royal Charlotte Bank
Grav. Anomaly (mGal)
c)

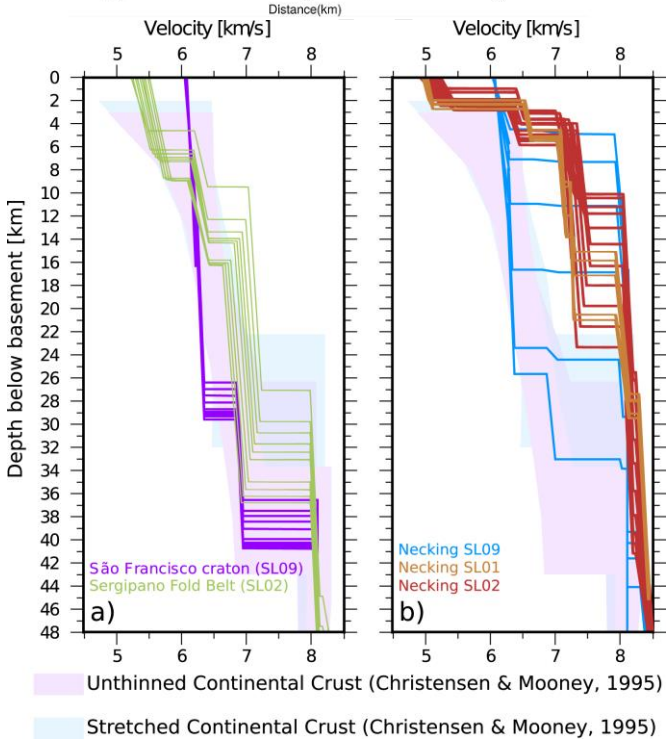
Velocity [km/s]
Velocity [km/s]
Depth below basement [km]
São Francisco craton (SL09)
Sergipano Fold Belt (SL02)
a)
Necking SL09
Necking SL01
Necking SL02
b)
Unthinned Continental Crust (Christensen & Mooney, 1995)
Stretched Continental Crust (Christensen & Mooney, 1995)

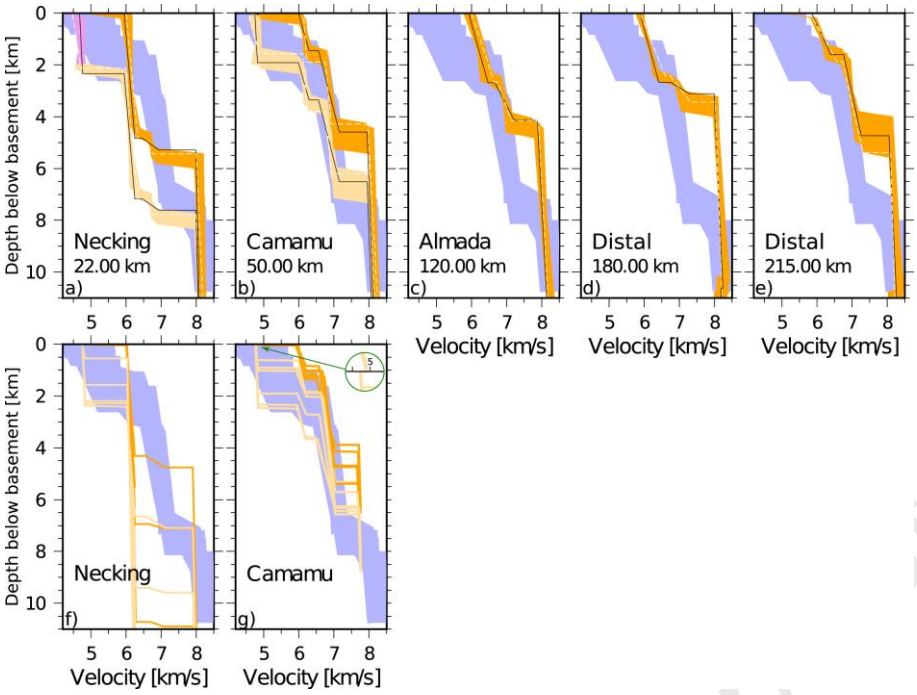

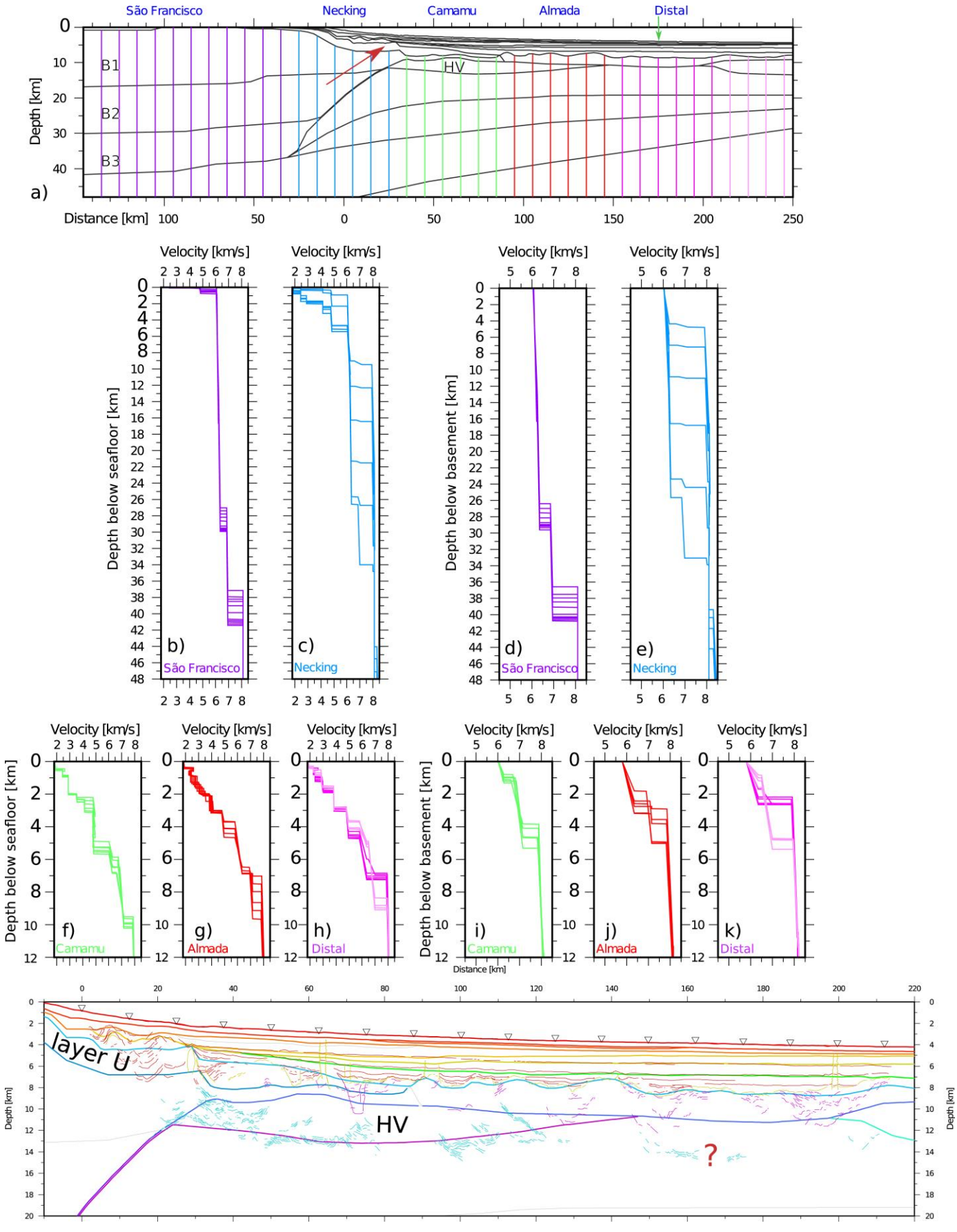
São Francisco
Necking
Camamu
Almada
Distal
B1
B2
B3
HV
Depth [km]
Distance [km]
a)
Velocity [km/s]
Depth below seafloor [km]
Depth below basement [km]
b) São Francisco
c) Necking
d) São Francisco
e) Necking
f) Camamu
g) Almada
h) Distal
i) Camamu
j) Almada
k) Distal
layer U
HV
?

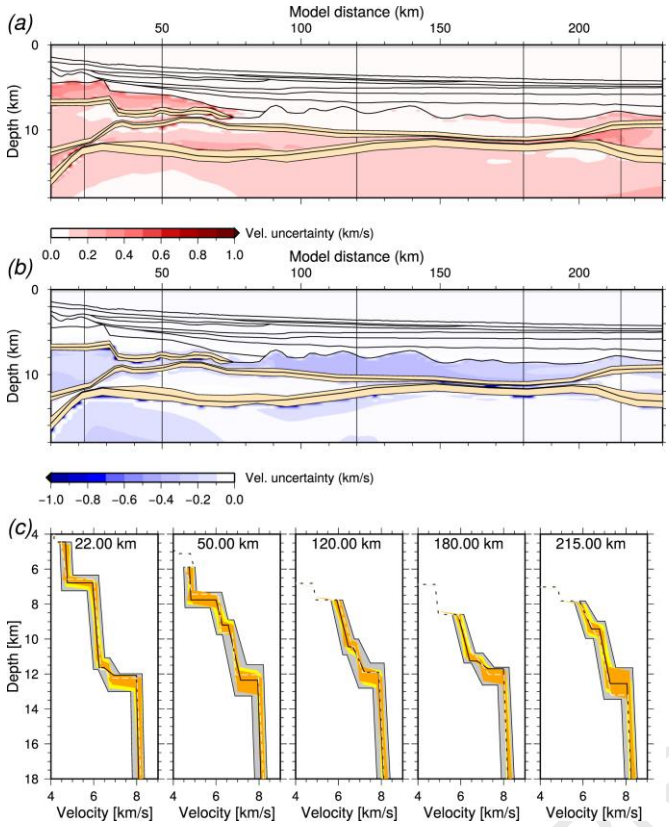

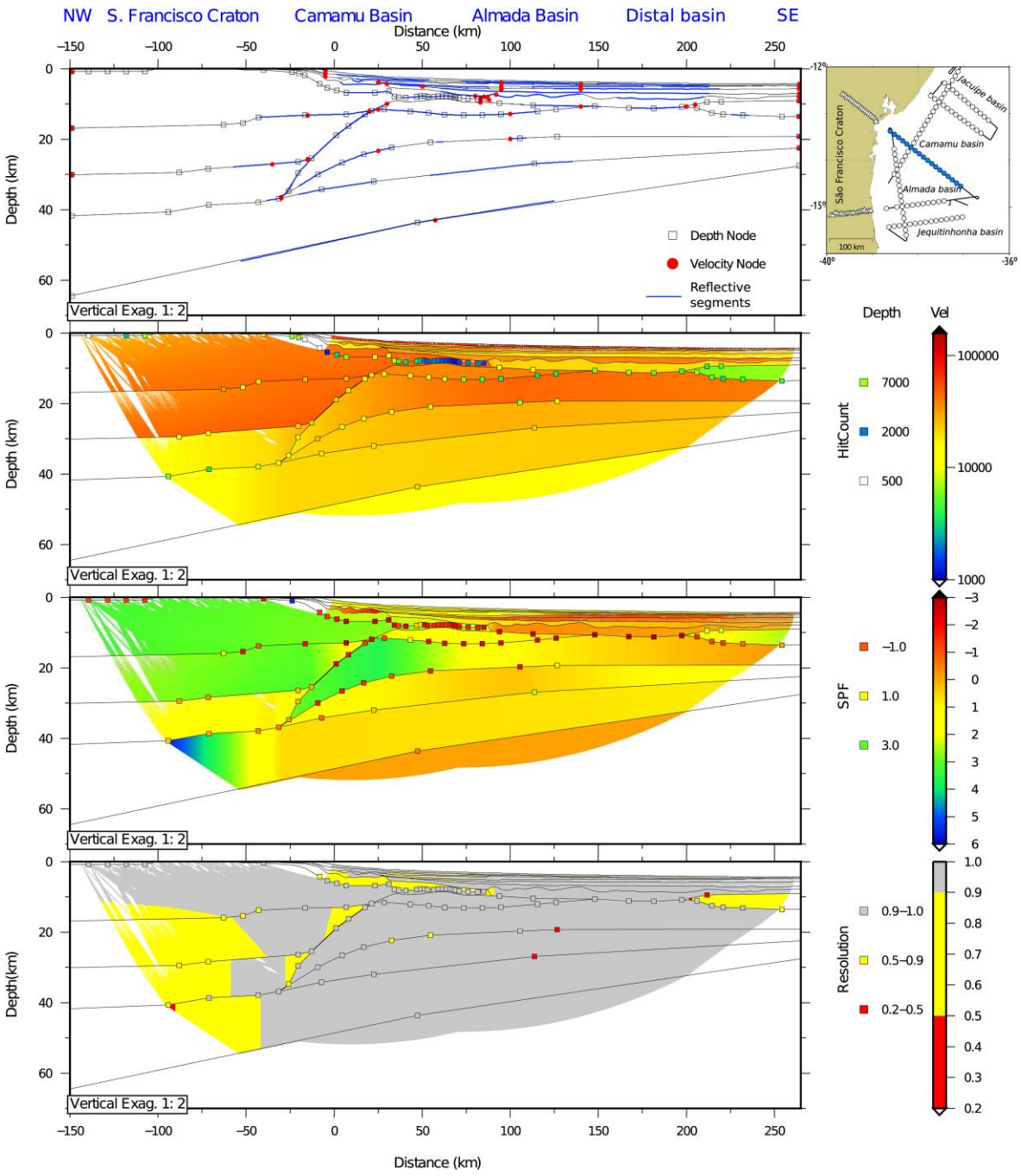
NW S. Francisco Craton
Camamu Basin
Almada Basin
Distal basin
SE
Distance (km)
Depth (km)
Depth Node
Velocity Node
Reflective segments
Vertical Exag. 1: 2
Jacuipe basin
Camamu basin
Almada basin
Jequitinhonha basin
São Francisco Craton
100 km
Depth
Vel
HitCount
7000
2000
500
100000
10000
1000
SPF
−1.0
1.0
3.0
Resolution
0.9–1.0
0.5–0.9
0.2–0.5

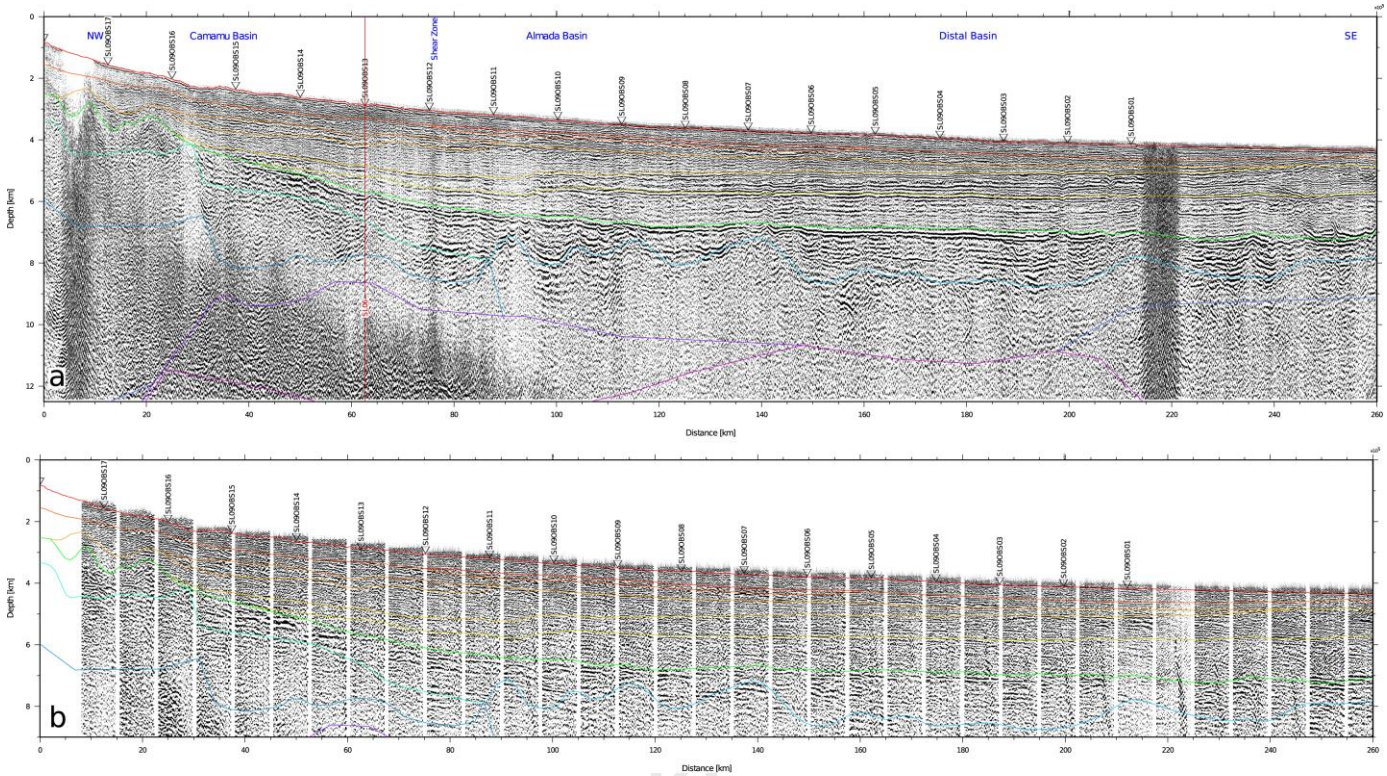

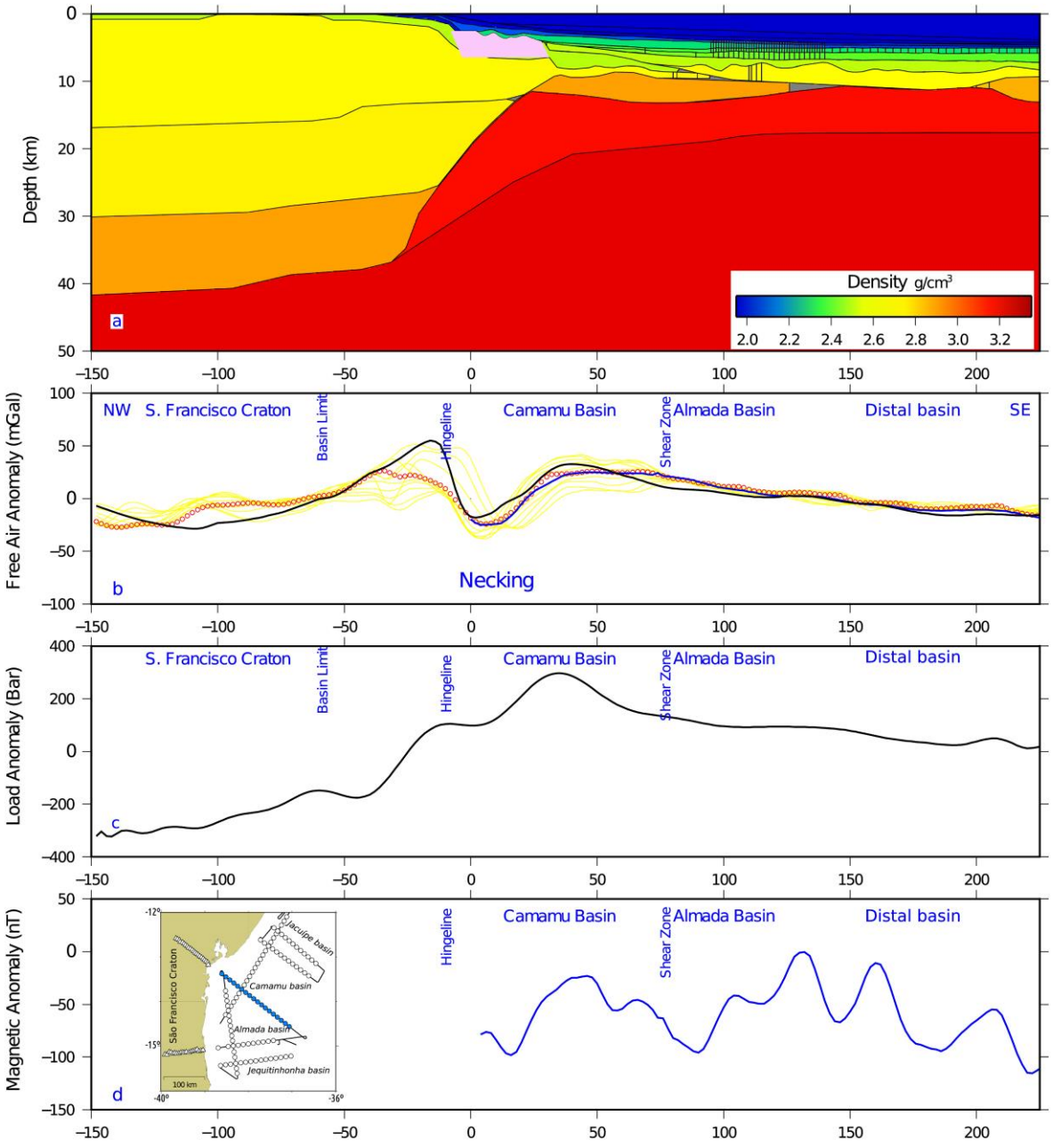
Depth (km)
Density g/cm³
2.0 2.2 2.4 2.6 2.8 3.0 3.2
a
NW S. Francisco Craton
Basin Limit
Hingeline
Camamu Basin
Shear Zone
Almada Basin
Distal basin
SE
Free Air Anomaly (mGal)
Necking
b
Load Anomaly (Bar)
c
Magnetic Anomaly (nT)
Jacuipe basin
Camamu basin
Almada basin
Jequitinhonha basin
São Francisco Craton
100 km
d

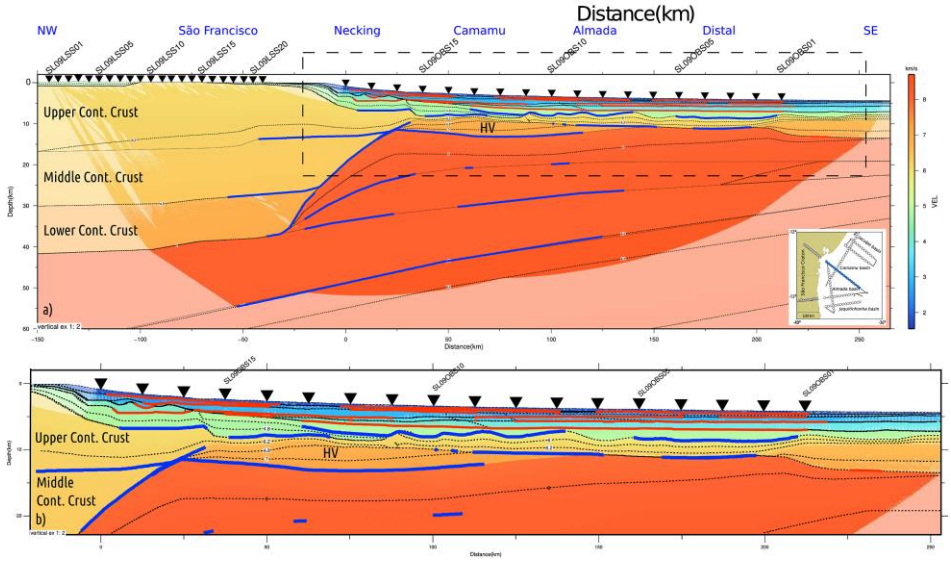
Distance(km)
NW
São Francisco
Necking
Camamu
Almada
Distal
SE
Upper Cont. Crust
Middle Cont. Crust
Lower Cont. Crust
HV
a)
Middle Cont. Crust
b)

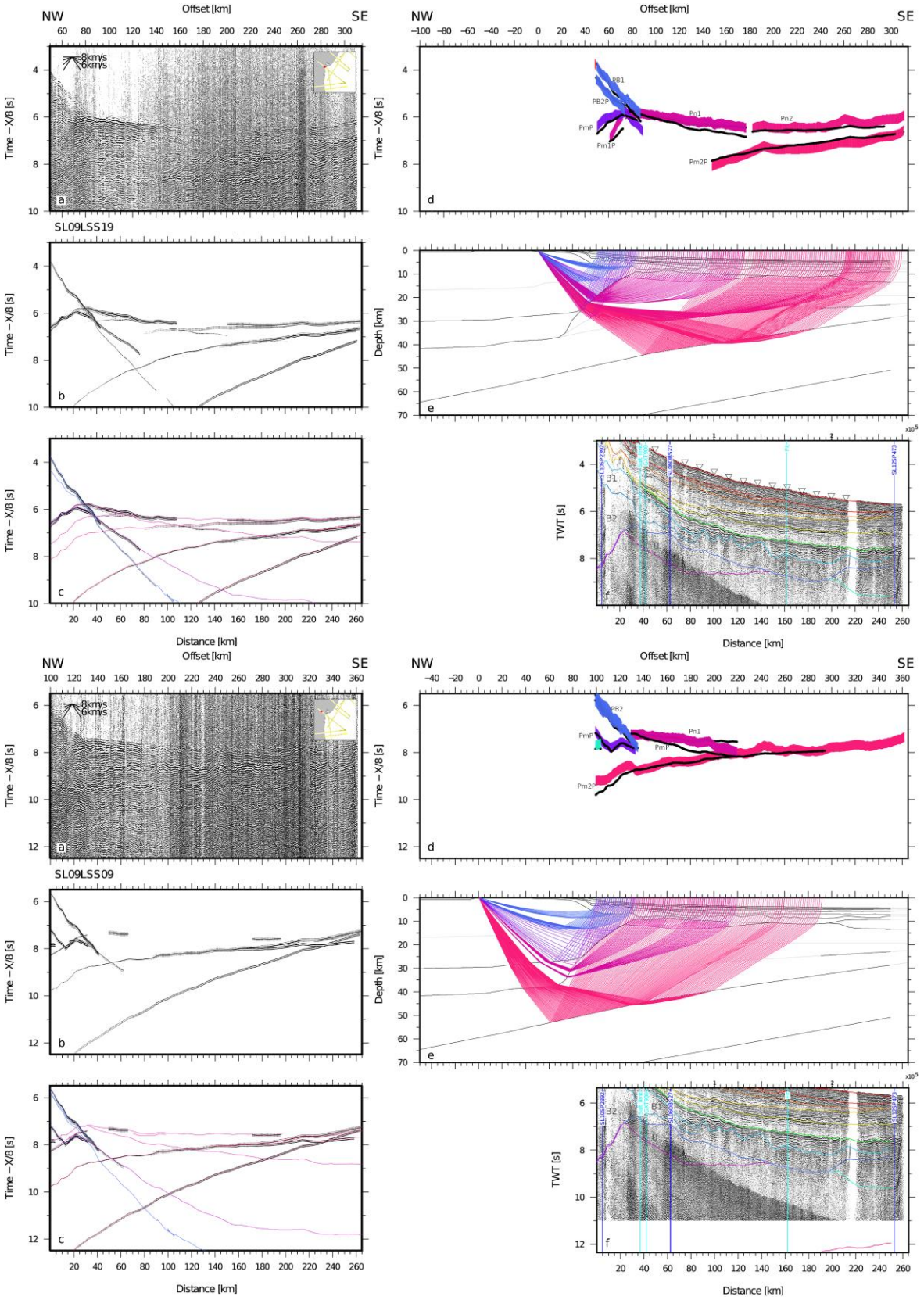
NW
SE
Offset [km]
8km/s
6km/s
Time − X/8 [s]
a
SL09LSS19
b
c
Distance [km]
d
PB1
PB2P
PmP
Pm1P
Pn1
Pn2
Pm2P
e
Depth [km]
f
TWT [s]
B1
B2
SL09LSS09

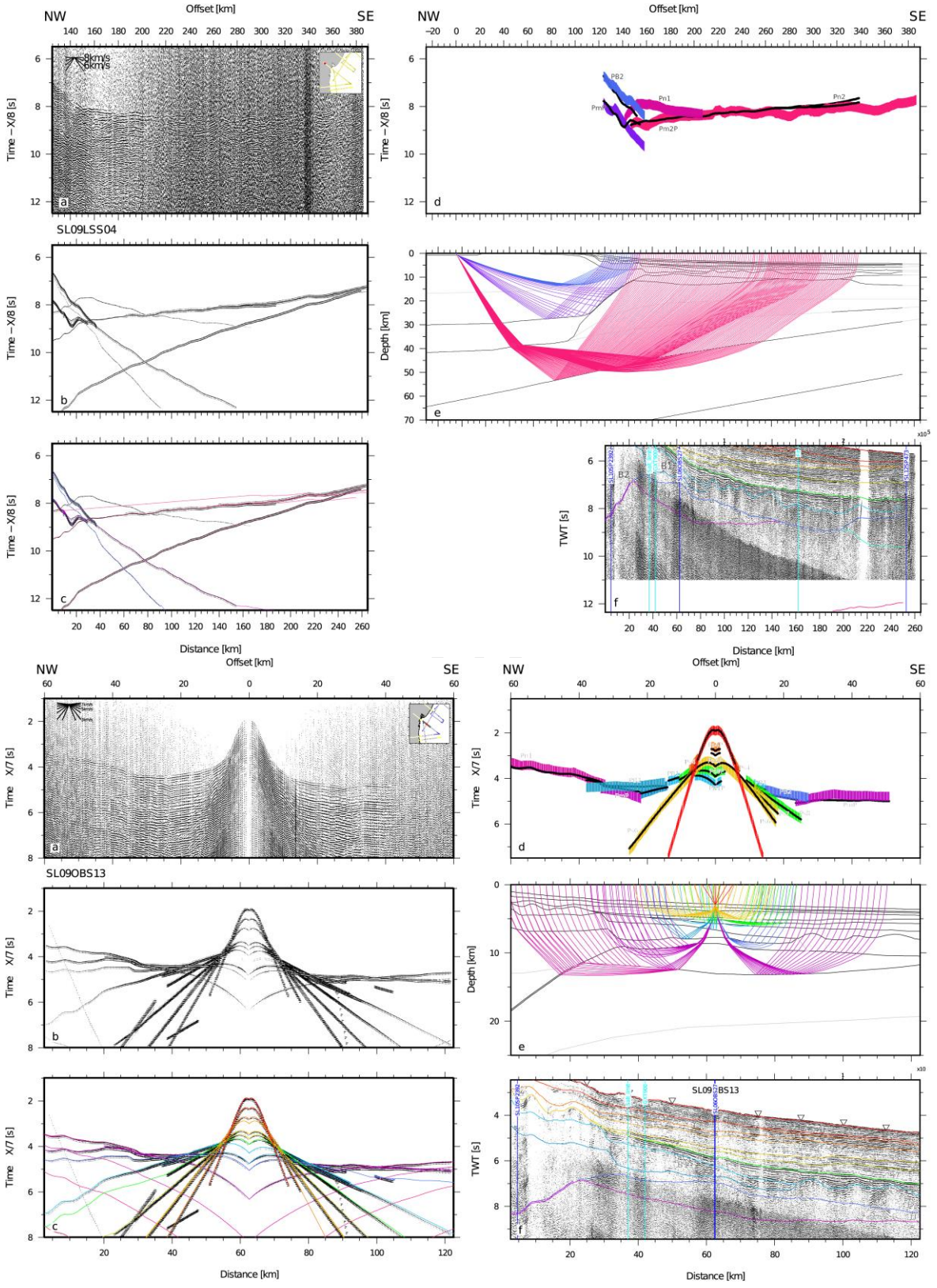
NW
SE
Offset [km]
8km/s
6km/s
Time − X/8 [s]
a
SL09LSS04
b
c
Distance [km]
d
PB2
Pn1
Pn2
Pm1P
Pm2P
e
Depth [km]
f
TWT [s]
B1
B2
Time X/7 [s]
SL09OBS13

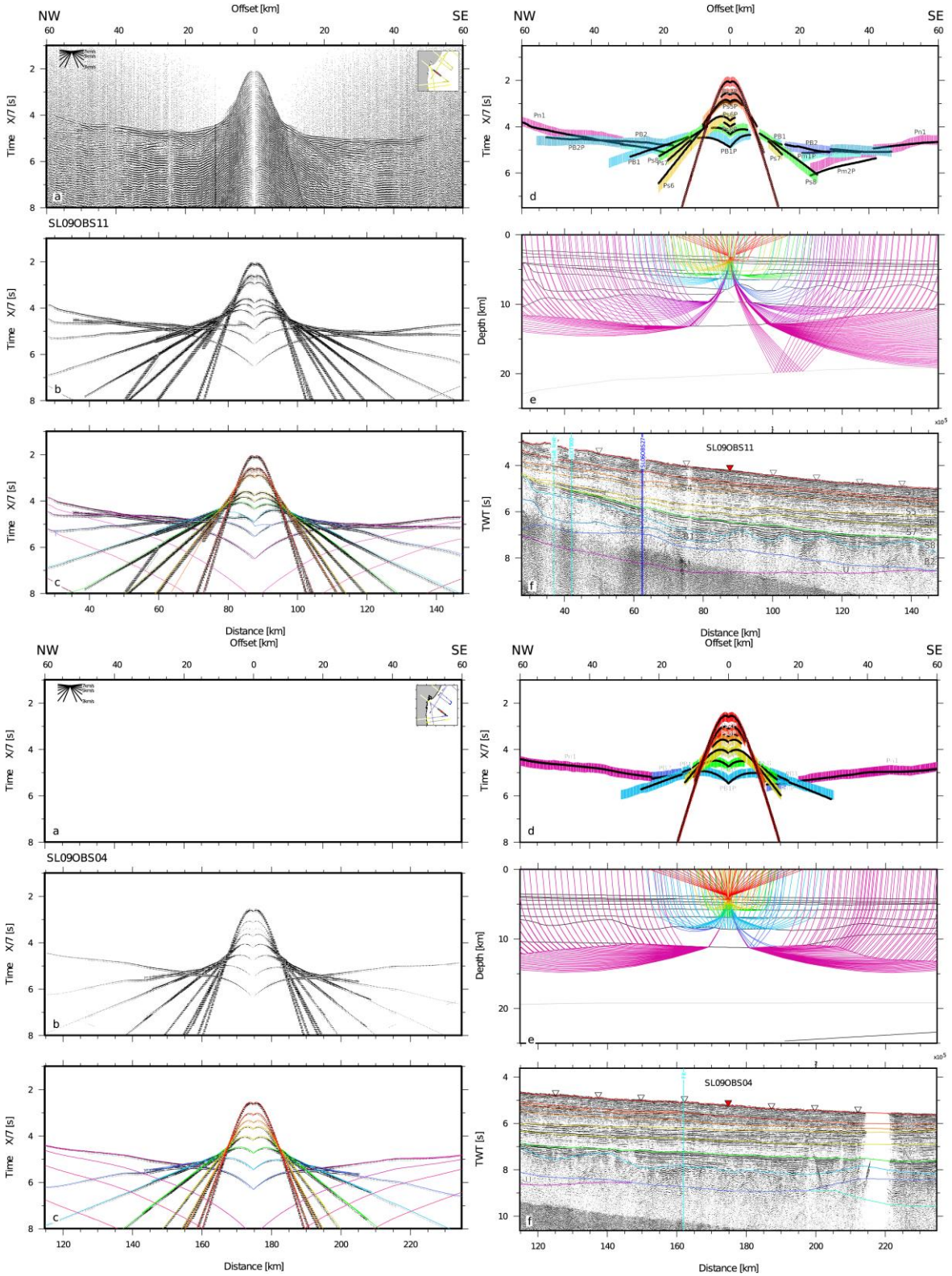
NW
SE
Offset [km]
Time X/7 [s]
SL09OBS11
Depth [km]
TWT [s]
Distance [km]
SL09OBS04

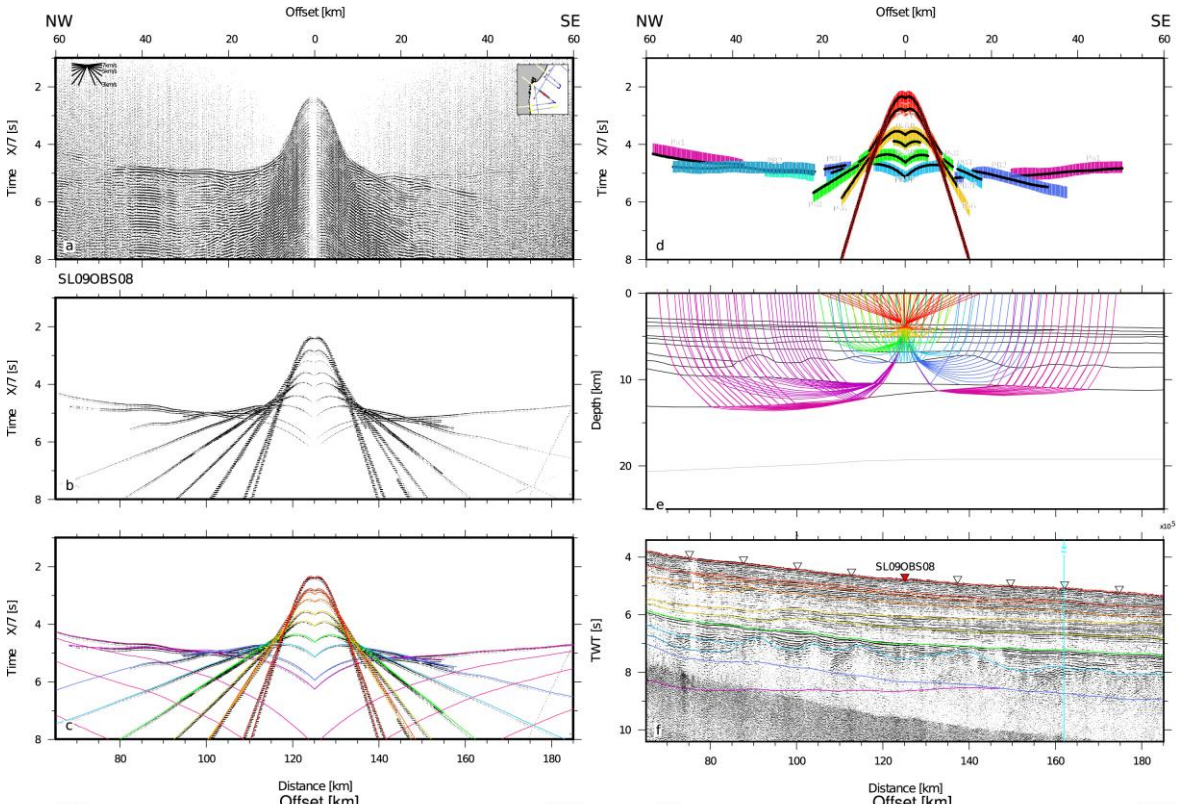
NW
SE
Offset [km]
Time – X/7 [s]
SL09OBS08
Depth [km]
TWT [s]
Distance [km]
a
b
c
d
e
f

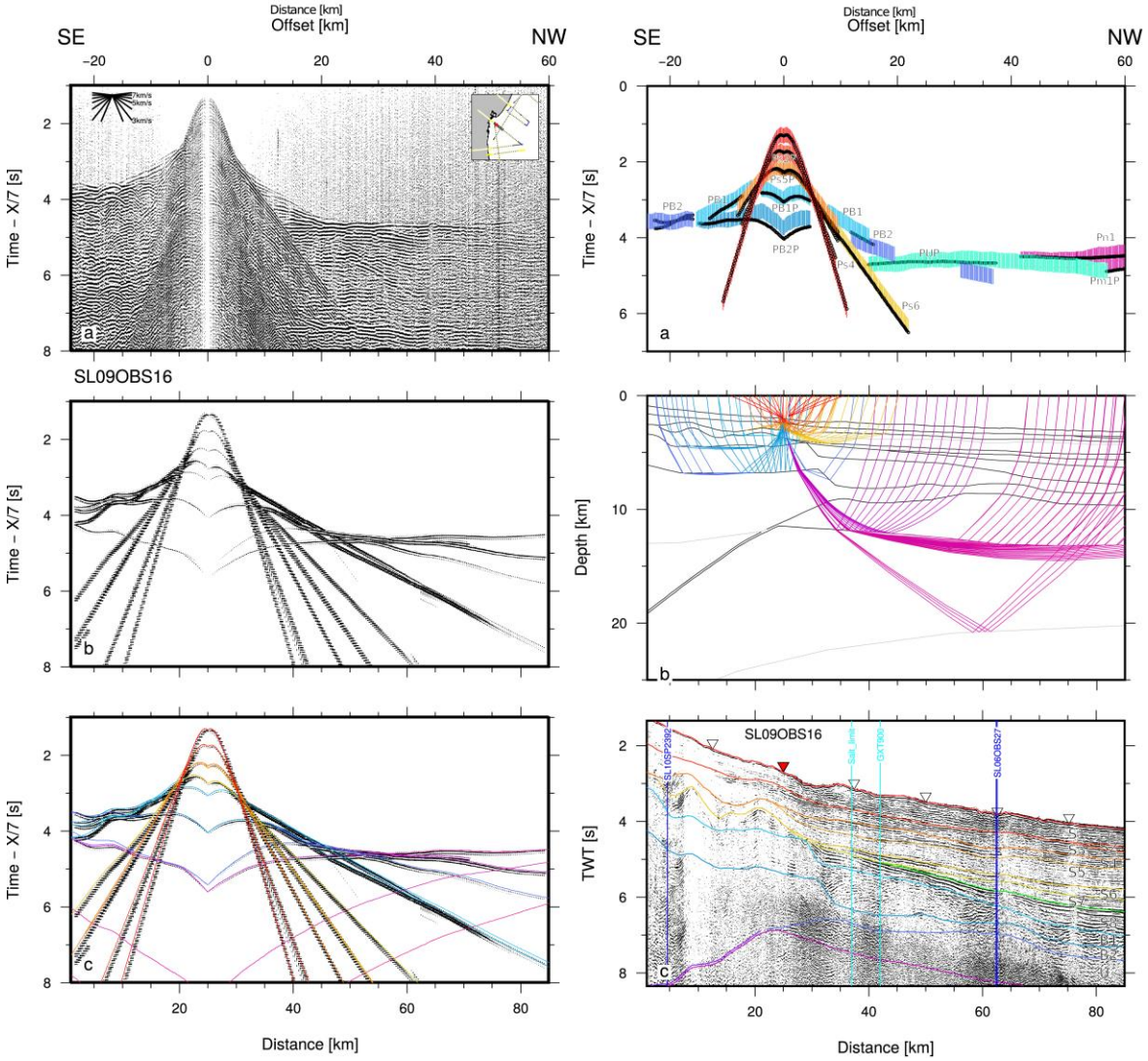
SE
NW
Offset [km]
Time – X/7 [s]
SL09OBS16
Depth [km]
TWT [s]
Distance [km]
PB2
PB1
PB1P
PB2P
Ps4
Ps6
Pn1
Pn1P
a
b
c

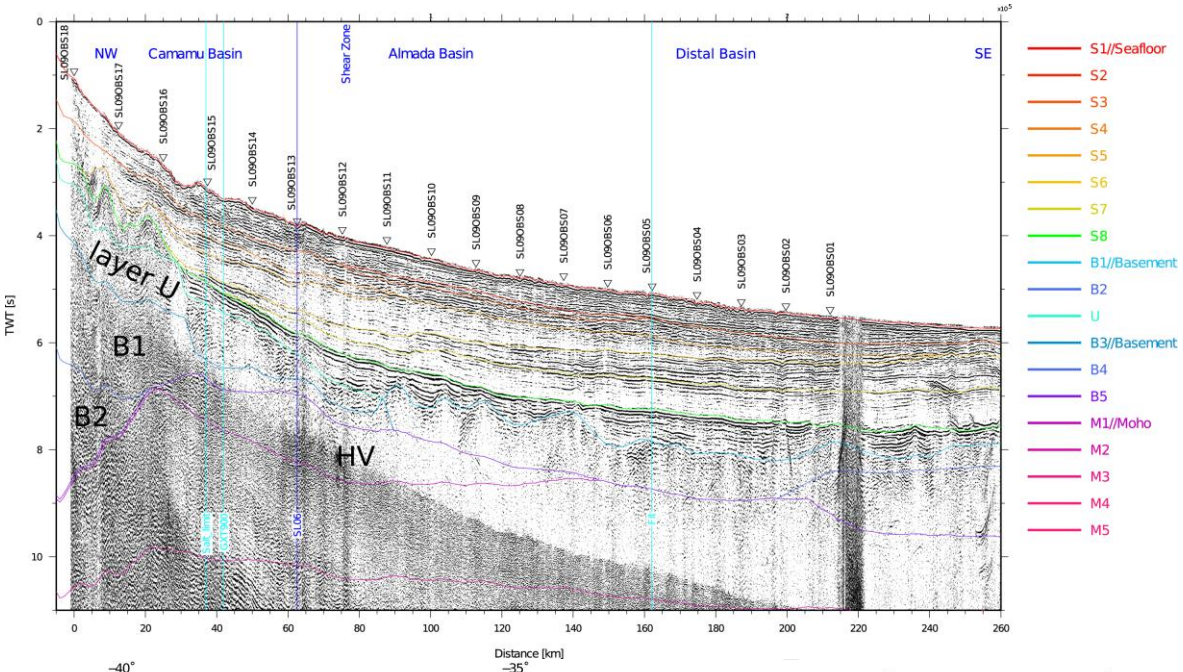
NW
Camamu Basin
Shear Zone
Almada Basin
Distal Basin
SE
layer U
B1
B2
HV
TWT [s]
Distance [km]
S1/Seafloor
S2
S3
S4
S5
S6
S7
S8
B1//Basement
B2
U
B3//Basement
B4
B5
M1//Moho
M2
M3
M4
M5

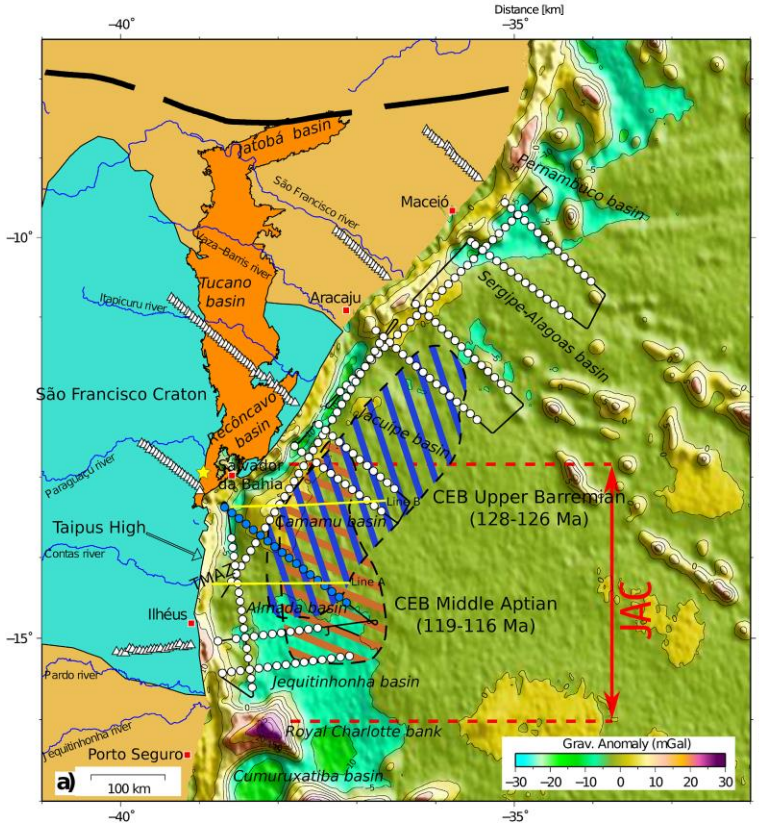
Jatobá basin
São Francisco river
Maceió
Pernambuco basin
Tucano basin
Aracaju
Sergipe-Alagoas basin
São Francisco Craton
Recôncavo basin
Jacuípe basin
Salvador da Bahia
CEB Upper Barremian (128-126 Ma)
Camamu basin
Taipus High
Contas river
TMA
Almada basin
CEB Middle Aptian (119-116 Ma)
JAC
Ilhéus
Pardo river
Jequitinhonha basin
Royal Charlotte bank
Jequitinhonha river
Porto Seguro
Cumuruxatiba basin
Grav. Anomaly (mGal)
a)
100 km

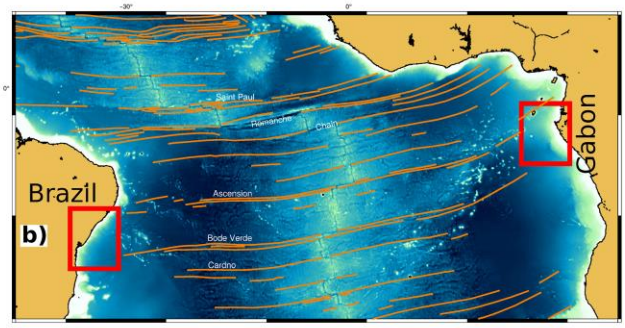
Brazil
Gabon
b)
Saint Paul
Fernando
Chain
Ascension
Bode Verde
Cadno

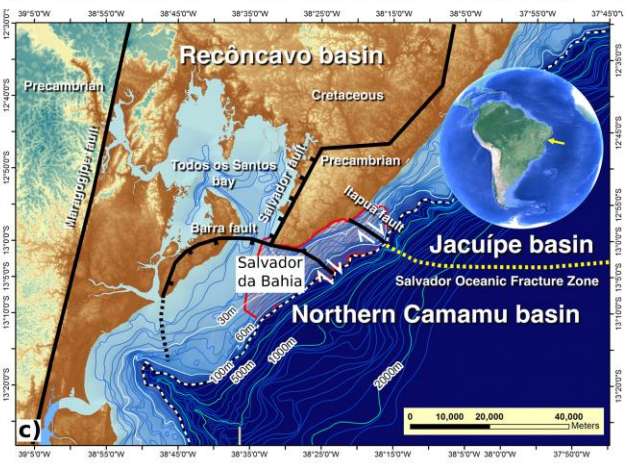
Recôncavo basin
Precambrian
Cretaceous
Precambrian
Todos os Santos bay
Salvador fault
Itapuã fault
Barra fault
Jacuípe basin
Salvador da Bahia
Salvador Oceanic Fracture Zone
Northern Camamu basin
30m
60m
100m
500m
1000m
2000m
c)
0 10,000 20,000 40,000 Meters

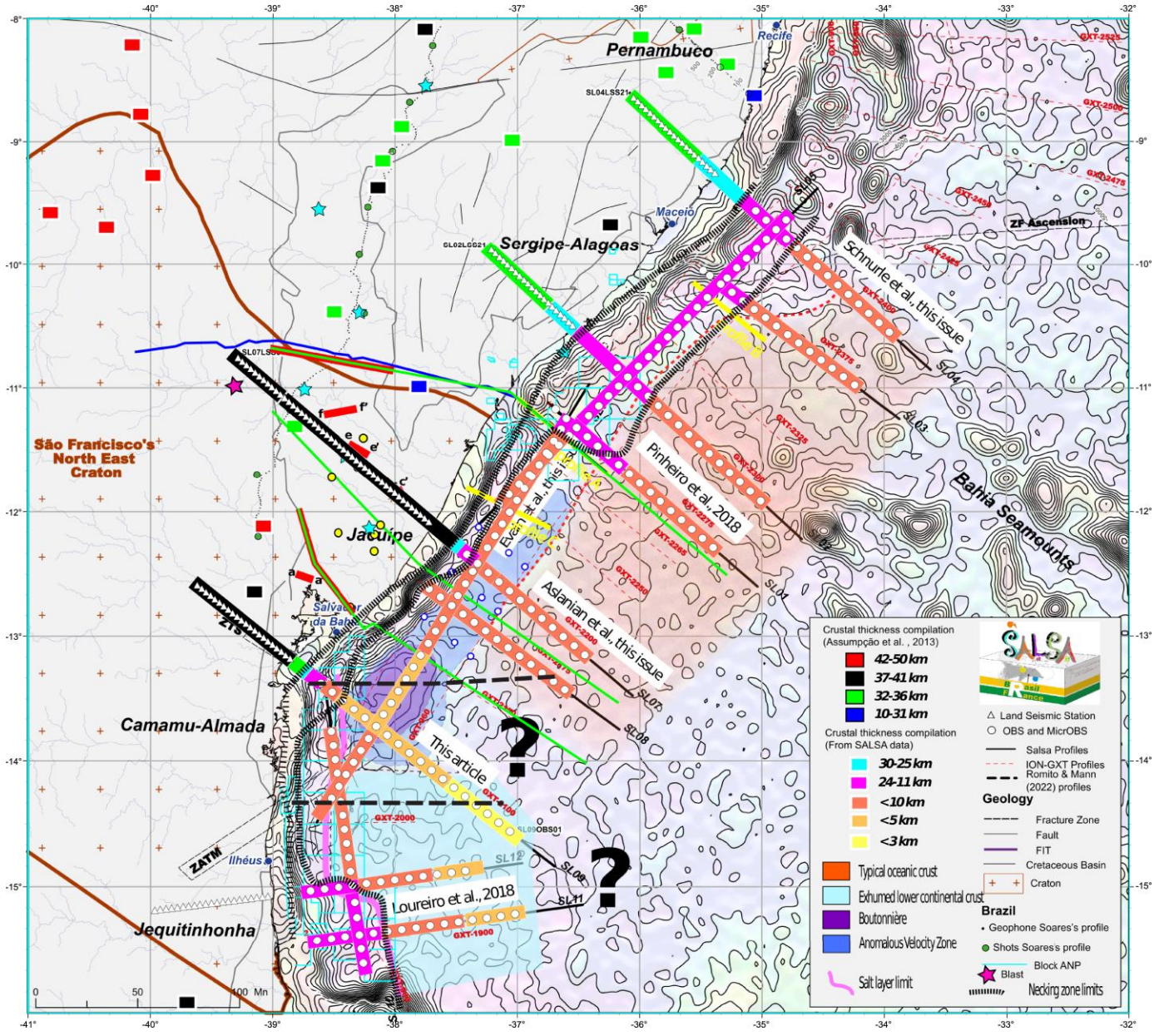
Pernambuco
Recife
Maceió
Sergipe-Alagoas
ZF Ascension
Schnurle et al., this issue
SL04
SL03
São Francisco's North East Craton
Jacuípe
Pinheiro et al., 2018
Evain et al., this issue
Bahia Seamounts
SL01
Aslanian et al., this issue
SL02
SL05
SL08
Camamu-Almada
This article
ZFS
ZATM
Ilhéus
SL12
SL09
SL11
Loureiro et al., 2018
Jequitinhonha
0
50
100 Mn
Crustal thickness compilation (Assumpção et al. , 2013)
42-50 km
37-41 km
32-36 km
10-31 km
Crustal thickness compilation (From SALSA data)
30-25 km
24-11 km
<10 km
<5 km
<3 km
Typical oceanic crust
Exhumed lower continental crust
Boutonnière
Anomalous Velocity Zone
Salt layer limit
Land Seismic Station
OBS and MicrOBS
Salsa Profiles
IGN-GXT Profiles
Romito & Mann (2022) profiles
Geology
Fracture Zone
Fault
FIT
Cretaceous Basin
Craton
Brazil
Geophone Soares's profile
Shots Soares's profile
Block ANP
Blast
Necking zone limits